NeuroImage 276 (2023) 120178

Contents lists available at ScienceDirect

NeuroImage

journal homepage: www.elsevier.com/locate/neuroimage

Novel multivariate methods to track frequency shifts of neural oscillations in EEG/MEG recordings

C. Vidaurre[a,b,c,*], K. Gurunandan[d,e], M. Jamshidi Idaji[f,g,h], G. Nolte[i], M. Gómez[c], A. Villringer[h], K.-R. Müller[f,g,j,k], V.V. Nikulin[h]

[a] Ikerbasque, Basque Foundation for Science, Plaza Euskadi 5, 48009 Bilbao, Spain
[b] Tecnalia Research and Innovation, Neuroengineering Group, Health Unit, Donostia, Spain
[c] Dept. of Statistics, Computer Science and Mathematics, Public University of Navarre, Pamplona, Spain
[d] MRC Cognition and Brain Sciences Unit, University of Cambridge, UK
[e] BCBL. Basque Center on Cognition, Brain and Language, Donostia-San Sebastián, Spain
[f] Machine Learning Group, Technische Universität Berlin, 10587 Berlin, Germany
[g] BIFOLD–Berlin Institute for the Foundations of Learning and Data, Germany
[h] Department of Neurology, Max Planck Institute for Human Cognitive and Brain Sciences, Leipzig, Germany
[i] Dept. of Neurophysiology and Pathophysiology, University Medical Center Hamburg-Eppendorf, Hamburg, Germany
[j] Department of Artificial Intelligence, Korea University, Anam-dong, Seongbuk-gu, Seoul 02841, South Korea
[k] Max Planck Institute for Informatics, Stuhlsatzenhausweg, 66123 Saarbrücken, Germany

ARTICLE INFO

Keywords:
Peak frequency
instantaneous frequency
spectral centroid
local frequency
multivariate methods
multimodal methods
multiple linear regression
correlation optimization
electroencephalography (EEG)
magnetoencephalography (MEG)
decomposition methods
source separation
spatial filters

ABSTRACT

Instantaneous and peak frequency changes in neural oscillations have been linked to many perceptual, motor, and cognitive processes. Yet, the majority of such studies have been performed in sensor space and only occasionally in source space. Furthermore, both terms have been used interchangeably in the literature, although they do not reflect the same aspect of neural oscillations. In this paper, we discuss the relation between instantaneous frequency, peak frequency, and local frequency, the latter also known as spectral centroid. Furthermore, we propose and validate three different methods to extract source signals from multichannel data whose (instantaneous, local, or peak) frequency estimate is maximally correlated to an experimental variable of interest. Results show that the local frequency might be a better estimate of frequency variability than instantaneous frequency under conditions with low signal-to-noise ratio. Additionally, the source separation methods based on local and peak frequency estimates, called LFD and PFD respectively, provide more stable estimates than the decomposition based on instantaneous frequency. In particular, LFD and PFD are able to recover the sources of interest in simulations performed with a realistic head model, providing higher correlations with an experimental variable than multiple linear regression. Finally, we also tested all decomposition methods on real EEG data from a steady-state visual evoked potential paradigm and show that the recovered sources are located in areas similar to those previously reported in other studies, thus providing further validation of the proposed methods.

1. Introduction

Neuronal oscillations have been functionally linked to many perceptual, motor, and cognitive functions (Blankertz et al., 2009; Buzsaki and Draguhn, 2004; Nierhaus et al., 2021; Vidaurre et al., 2020). While a majority of previous studies focused primarily on the relevance of oscillatory amplitude to these diverse functions, there is a growing understanding that the frequency of oscillations is also important for the functioning of large-scale neuronal dynamics at rest and during different tasks (Gammaitoni and Nov, 0000; Mierau et al., 2017; Sutherland et al., 2009; Tuckwell et al., 2009).

Understanding brain function requires the investigation of neuronal activity at different spatio-temporal scales, ranging from microseconds of individual spiking neurons to minutes or even hours of sleep recordings (e.g. obtained with electroencephalography, EEG). Such investigation has become increasingly popular due to the study of temporal fluctuations of peak and instantaneous frequency estimates in oscillatory activity at specific frequency bands. A special emphasis on alpha oscillations exists in the literature because it represents the most salient rhythmic phenomenon in human EEG and magnetoencephalographic (MEG) recordings. The review presented in Mierau et al. (2017) discusses several phenomena that cause a temporal shift of the alpha peak

* Corresponding author.
E-mail address: carmen.vidaurre@tecnalia.com (C. Vidaurre).

https://doi.org/10.1016/j.neuroimage.2023.120178.
Received 16 May 2022; Received in revised form 9 March 2023; Accepted 17 May 2023
Available online 25 May 2023.

frequency (APF). For example, APF is age dependent, demonstrating an increase during childhood, stabilizing during adulthood, and then decreasing with age or due to neurological pathologies such as Alzheimer's disease. Also, APF shifts are dependent on the individual's state. For instance, an APF decrease has been observed with emotions such as fear or sorrow, whereas joy or anger resulted in an increase in APF (Hülsdünker et al., 2016). It was also shown that APF decreases when the state of consciousness is lower (Lechinger et al., 2013).

Moreover, a number of studies suggest that peak frequency changes are a function of task demand or input intensity. For example, the performance of working memory tasks showed to accelerate APF according to the intensity of the task (a higher load is related to a higher APF) (Haegens et al., 2014; Maurer et al., 2015). Higher APF has been previously associated with a more refined sampling of visual information (Samaha and Postle, 2015). An increase in APF has been also observed during demanding physical tasks (Hülsdünker et al., 2016) due to increased attention and somatosensory input. Recently, Mahjoory et al. (2020) showed a significant relationship between the gradient of the APF along the posterior-anterior axis and its correspondence to cortical thickness in resting MEG from healthy participants. This relation was connected to the global cortical hierarchy from early sensory to higher-order areas. In another recent work, Lundqvist et al. (2020), using neuronal spikes and local field potentials simultaneously recorded from monkeys, showed that theta, alpha, beta, and gamma rhythms have similar functions across the cortex, and their (peak) frequencies in all bands increase with the cortical hierarchy. Additionally, Nelli et al. (2017) showed that fluctuations of instantaneous frequency predict alpha amplitude in a visual discrimination task, thus concluding that they are not independent. Finally, Valdés-Hernández et al. (2010) showed that alpha peak inter-individual differences are related to brain connectivity variations. Furthermore, an increasing number of experimental results clearly indicate that peak frequency shifts are a common occurrence in brain signals, not limited to particular tasks (Benwell et al., 2019). However, the link between peak changes and neural processing states is still poorly understood.

To a large extent, the investigation of peak frequency fluctuations is challenging because of methodological reasons. First, frequency fluctuations are difficult to estimate due to the often low signal-to-noise ratio of EEG signals, especially in higher frequency bands such as beta and gamma, which are commonly analyzed in neuroscientific experiments. Moreover, due to volume conduction and source mixing, sources related to frequency shifts cannot be directly observed at the sensor level. Second, there is a general lack of methods that allow extracting brain sources related to changes in peak or instantaneous frequency characteristics. Usually, correlations are performed in sensor space. However, sensor space approaches present several drawbacks, including a lack of interpretability due to the mixing of different sources and disregarding the generative model of neuroimaging signals (Haufe et al., 2014b). These shortcomings can be addressed by methods that decompose multivariate EEG/MEG data into a set of source components, where the decomposition is based on the information contained in a target variable. Finally, two different estimates related to frequency fluctuations are studied as reflecting a similar process - peak and instantaneous frequency. However, they are generally not equivalent, rendering general statements about peak frequency fluctuations rather challenging.

In this work, we shortly explain the relation between different frequency shift estimates and then propose different methods to find brain sources whose frequency measure of interest is maximally correlated to an external or internal (experimental) variable. This variable can be related to the previously discussed user state, sensory or motor input/output (Dähne et al., 2014b; Maurer et al., 2015; Mierau et al., 2017; Samaha and Postle, 2015; Vidaurre et al., 2019a; 2013). In this context, our methods result in a spatial filter that maximizes the linear correlation between the target variable and the measure of the frequency shift of the spatially filtered signal. We then demonstrate the viability of the methods using extensive simulations based on a realistic head model. We also apply our methods to real EEG data relating to steady-state visual evoked responses. Finally, we discuss the obtained results and provide considerations for the application and limitations of the proposed methods.

2. Methods and experimental data

2.1. Notation

We denote vectors with boldface lower-case letters (e.g. $\boldsymbol{x}$) and matrices with boldface capital letters (e.g. $\boldsymbol{X}$). Scalars are indicated by regular letters (e.g. x). Fourier transformed vector time series are represented by $\boldsymbol{\mathcal{X}}(f)$.

The imaginary number $\sqrt{-1}$ is denoted by j, and the complex conjugate of a complex number $z \in \mathbb{C}$ is denoted by z^*. The operators that return the real part, imaginary part, the absolute value, and the argument of a complex number are denoted by $\Re\{.\}$, $\Im\{\}$, $|.|$, and $\arg(.)$, respectively. The subscript a denotes the analytic signal built using Hilbert transform. Formally, if $x(t)$ is a real valued signal with $H\{x(t)\}$ being its Hilbert transform, the corresponding analytic signal is $x_a(t) = x(t) + jH\{x(t)\}$.

2.2. The generative model of EEG/MEG data

Both EEG and MEG are non-invasive techniques to measure brain activity. Despite both techniques having an excellent temporal resolution in the order of milliseconds, their spatial resolution is heavily compromised by volume conduction and signal mixing, leading to the detection of activity from even one source in almost all sensors (Schaworonkow and Nikulin, 2022). For frequencies under 1 kHz, this superposition is linear and instantaneous, thus it is possible to find a linear model of EEG/MEG data (Baillet et al., 2001; Hashemi et al., 2021; Haufe et al., 2014b; Nunez and Srinivasan, 2006; Parra et al., 2005) as the following:

$$\mathbf{x}(t) = \mathbf{A}\mathbf{s}(t) + \boldsymbol{\epsilon}(t) \tag{1}$$

where $\mathbf{x}(t) \in \mathbb{R}^{N_x}$ is a vector of data measured by N_x sensors at time t, $\mathbf{s}(t) \in \mathbb{R}^{N_s}$ is a vector of N_s source signals, and the matrix $\mathbf{A} \in \mathbb{R}^{N_x \times N_s}$ is the mixing matrix with its i-th column being the spatial activation pattern of the i-th source. Finally, $\boldsymbol{\epsilon}(t)$ represents the additive noise. Often, the noise part is discarded and Equation 1 can be rewritten as:

$$\mathbf{x}(t) = \boldsymbol{A}\mathbf{s}(t) \tag{2}$$

Equation 2 is generally denoted as the *forward model* of the EEG/MEG. The objective of many neuroimaging methods is to (semi-)blindly decompose multi-channel data to the source signals and their activation patterns according to this model. In most of source separation techniques, one is not interested in building the whole generative model for the observed data, as in Equation 2. Rather, there is an interest in the extraction of a specific type of source with a special characteristic. Therefore, the separation of the sources is done by estimating a linear subspace, on which the projections of the measured data $\mathbf{x}(t)$ are estimations of the sources of interest. The linear mapping from the subspace of the observed data to the latent source signals is a matrix $\boldsymbol{W} \in \mathbb{R}^{N_x \times N_s}$, whose columns are spatial filters that extract the estimates of the specific sources as the following:

$$\hat{\mathbf{s}}(t) = \boldsymbol{W}^\top \mathbf{x}(t) \tag{3}$$

The above equation is usually referred to as the *backward model*. Furthermore, these linear models can be written in the frequency domain. Applying a Fourier transform to both sides of Equations 2 and 3, they can be written as:

$$\boldsymbol{\mathcal{X}}(f) = \boldsymbol{A}\boldsymbol{\mathcal{S}}(f) \tag{4}$$

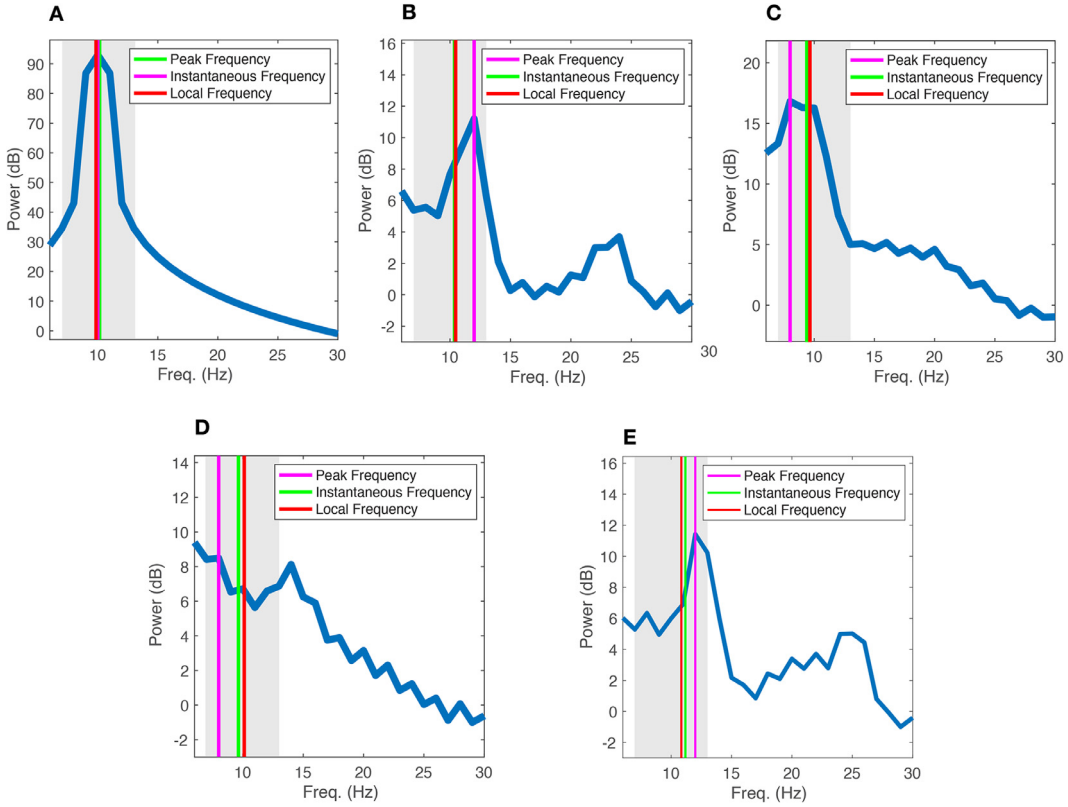

Fig. 1. Exemplar power spectra and the estimated peak, local, and instantaneous frequencies. (A) a simulated spectrum with a symmetric spectral peak at 10 Hz, for which f_{peak}, f_{loc} and $\langle f_i \rangle$ coincide. Other panels: power spectral density of real EEG data of one channel where f_{peak} does not coincide with f_{loc} and $\langle f_i \rangle$. Note that f_{loc} and $\langle f_i \rangle$ estimates have very similar, almost coincident, values. The light gray shaded area indicates the bandwidth in which frequency estimates were computed.

$$\hat{\boldsymbol{S}}(f) = \boldsymbol{W}^{\top} \boldsymbol{\mathcal{X}}(f) \tag{5}$$

with $\boldsymbol{\mathcal{X}}(f)$ and $\hat{\boldsymbol{S}}(f)$ being the Fourier representations of the time series $\mathbf{x}(t)$ and $\hat{\mathbf{s}}(t)$ at frequency f.

2.3. Definitions: instantaneous, local, and peak frequency

In neural data analyses two measures are commonly used to investigate frequency changes in oscillatory signals. One is the peak frequency (f_{peak}) estimate. This is the frequency location of the spectral peak of the frequency domain signal in the band of interest. The second frequency measure is the instantaneous frequency (f_i), which is defined in the time domain as:

$$f_i(t) = \frac{1}{2\pi} \frac{d}{dt} \arg\left(x_a(t) \right) \tag{6}$$

where $x_a(t) \in \mathbb{C}$ is the complex analytic signal of $x(t)$.

$f_i(t)$ is known to be highly susceptible to noise, especially when the signal-to-noise ratio (SNR) is low, as in EEG data (Sameni and Seraj, 2017). Some alternatives have been suggested to ameliorate this problem. For example, Cohen (2014) suggested using a median filter that has a smoothing/averaging effect on the instantaneous estimates. In the same spirit, let us define the following weighted average of $f_i(t)$ over time:

$$\langle f_i \rangle = \frac{\int_{-\infty}^{+\infty} f_i(t) |x_a(t)|^2 dt}{\int_{-\infty}^{+\infty} |x_a(t)|^2 dt} \tag{7}$$

where the operator $\langle . \rangle$ is the average operator. Equation 7 is also a smooth estimate of $f_i(t)$ thanks to averaging. Interestingly, $\langle f_i \rangle$ is equal to the local frequency (f_{loc}) or average frequency of the spectrum (Boashash, 1992), defined as:

$$f_{\text{loc}} = \frac{\int_{-\infty}^{+\infty} f |\mathcal{X}_a(f)|^2 df}{\int_{-\infty}^{+\infty} |\mathcal{X}_a(f)|^2 df} \tag{8}$$

where $\mathcal{X}_a(f)$ is the Fourier representation of the analytic signal $x_a(t)$.

The complete derivation of Equations 7 and 8 is available in (Ville, 1948). Equation 8, is a power spectral centroid, thus it shows that when the power spectrum in the band of interest has a symmetric peak, f_{loc} will be located at its maximum value (at the peak), and f_{loc} and f_{peak} will coincide. However, this is hardly ever the case in practice, because the EEG power spectrum follows a power-law decay and the spectral peaks are quite often asymmetric. As an illustration, the top left panel of Fig. 1 shows an artificially generated symmetric peak around the frequency band of interest (7 to 13 Hz), where all frequency estimates (f_{peak}, f_{loc} and $\langle f_i \rangle$) coincide. The remaining panels in the same figure show different examples on real EEG data where f_{peak}, f_{loc} and $\langle f_i \rangle$ do not coincide. One can also observe that, the time averaged f_i and f_{loc} are very similar.

2.4. Problem Formulation

In this paper, the goal is to extract source signals from multi-channel data whose f_{peak}, f_{loc} or $\langle f_i \rangle$ are maximally co-modulated (i.e. they are maximally (anti)-correlated) with another experimental variable. This can be an external variable like the subject's demographics or behavior, or an internal one, for instance, amplitude-envelope fluctuations of brain oscillatory activities.

Assume that the multi-channel data $\mathbf{x}(t)$ are segmented to n_e epochs $\mathbf{x}_n(t), n = 1, \cdots, n_e$ - the subscript n denoting the n-th epoch. Additionally, there is a target variable z_n associated with each epoch of data. In this work, we aim at finding one or more latent sources such that their instantaneous, local, or peak frequency is maximally correlated with the target variable. For simplicity of the formulation, let's assume we want to find one latent source. Formally, we want to solve a backward problem $s_n(t) = \mathbf{w}^T\mathbf{x}_n(t)$ for each epoch of data. Note that the spatial filter $\mathbf{w}$ is the same for all epochs of data. We use a least square optimization for formulating our problem as the following:

$$\min_{\mathbf{w}} \sum_{n=1}^{n_e} \Big(z_n - \beta f_{\text{src}}\big(\mathbf{w}\mathbf{x}_n(t)\big)\Big)^2 \tag{9}$$

where the source frequency $f_{\text{src}}(\mathbf{w}\mathbf{x}_n)$ can be either $\langle f_i \rangle$, f_{loc} or f_{peak} of the projection of the multi-channel data on the subspace defined by $\mathbf{w}$, that is $s_n(t) = \mathbf{w}\mathbf{x}_n(t)$.

In the following three sections, we formulate the instantaneous, local, and peak frequency as a function of the spatial filter $\mathbf{w}$ and multi-channel data $\mathbf{x}_n(t)$.

2.5. Instantaneous Frequency Decomposition, IFD

The instantaneous frequency $f_i(t)$ of $\mathbf{s}(t) = \mathbf{w}^T\mathbf{x}(t)$ can be computed sample by sample as in Equation 6. It can be shown that $f_i(t, \mathbf{w})$ can be obtained from the following equation (details are provided in Appendix A):

$$f_i(t, \mathbf{w}) = \frac{1}{2\pi}\Im\left\{\frac{\mathbf{w}^\top \frac{d\mathbf{x}_a(t)}{dt}\mathbf{w}^\top\mathbf{x}_a(t)^{\text{H}}}{\mathbf{w}^\top\mathbf{x}_a(t)\mathbf{x}_a(t)^{\text{H}}\mathbf{w}}\right\} \tag{10}$$

where $^{\text{H}}$ denotes the conjugate transpose.

In practice, one can avoid computing the numerical time derivative of $\mathbf{x}_a(t)$ by writing it in terms of its discrete Fourier transform (DFT):

$$\mathbf{x}_a(t) = \frac{1}{T}\sum_{f=f_1}^{f_2} \mathcal{X}_a(f) e^{\frac{j2\pi ft}{T}} = \frac{1}{T}\sum_{f=f_1}^{f_2} 2\mathcal{X}(f) e^{\frac{j2\pi ft}{T}} \tag{11}$$

where $\mathcal{X}(f)$ is the DFT of the multi-channel signal $\mathbf{x}(t)$ and T is the number of available time samples. Then, its corresponding time derivative is:

$$\frac{d\mathbf{x}_a(t)}{dt} = \frac{j4\pi}{T^2}\sum_{f=f_1}^{f_2} f\mathcal{X}(f) e^{\frac{j2\pi ft}{T}} \tag{12}$$

Thus, in order to obtain $f_i(t, \mathbf{w})$ we substitute $\mathbf{x}_a(t)$ and $\frac{d\mathbf{x}_a(t)}{dt}$ in Equation 10 with Equations 11 and 12.

Finally, the estimation of $f_i(t, \mathbf{w})$ can be improved by averaging its values over windows of data. In this case, we average $f_i(t, \mathbf{w})$ over time within each trial. If a trial consists of N samples, in the n-th epoch we obtain:

$$\langle f_i(n, \mathbf{w})\rangle = \frac{\sum_{t=1}^{t=N} f_i(t, \mathbf{w})}{N} \tag{13}$$

Note that this averaged estimate of $f_i(t)$ is not the same as the one in Equation 7, where the average was weighted with the squared signal values. The estimate of Equation 7 coincides with f_{loc}, for which we provide a decomposition approach in the next section. Thus, for IFD we selected the usual mean estimate and, from now on, $\langle f_i \rangle$ refers to the estimate in Equation 13.

2.6. Local Frequency Decomposition, LFD

f_{loc} (Boashash, 1992) is an estimate of the first central moment of a frequency distribution normalized by its energy (see Equation 8), sometimes also denominated spectral centroid. We show in Appendix B that f_{loc} can be computed for the frequency band $[f_1, f_2]$ Hz from the following equation:

$$f_{\text{loc}}(n, \mathbf{w}) = \frac{\mathbf{w}^\top\left(\sum_{f=f_1}^{f_2} f\,\Re\{\mathcal{X}(f,n)\mathcal{X}^{\text{H}}(f,n)\}\right)\mathbf{w}}{\mathbf{w}^\top\left(\sum_{f=f_1}^{f_2} \Re\{\mathcal{X}(f,n)\mathcal{X}^{\text{H}}(f,n)\}\right)\mathbf{w}} \tag{14}$$

2.7. Peak Frequency Decomposition, PFD

Computationally, it is possible to approach f_{peak} using a slight modification of the f_{loc} definition such that in Equation 8 the term $|\mathcal{X}_a(f)|$ is raised to the power $p > 2$. Then, the weighting of the peak frequency will be *much* larger than other frequencies in Equation 14 and therefore, f_{loc} moves closer to f_{peak} of the power spectrum computed using $|\mathcal{X}_a(f)|^p$. Fig. 2 shows an example of this behavior, where f_{loc} and f_{peak} are computed with the power spectrum (PS, left panel), with $p = 5$ (middle) $p = 15$ (right). As the exponent increases, the estimates of f_{loc} and f_{peak} get closer to each other.

Thus, an approximation of f_{peak} can be found using the formulation of f_{loc} in Equation 8 by substituting $|\mathcal{X}_a(f)|^2$ by $|\mathcal{X}_a(f)|^p$. Therefore, Equation 14 is changed to the following:

$$f_{\text{peak}}(n, \mathbf{w}) \approx \frac{\sum_{f=f_1}^{f_2} f\left(\mathbf{w}^\top\Re\{\mathcal{X}(f,n)\mathcal{X}^{\text{H}}(f,n)\}\mathbf{w}\right)^p}{\sum_{f=f_1}^{f_2}\left(\mathbf{w}^\top\Re\{\mathcal{X}(f,n)\mathcal{X}^{\text{H}}(f,n)\}\mathbf{w}\right)^p} \tag{15}$$

with $p \gg 2$. The bigger the exponent p, the closer the result of Equation 15 to the actual f_{peak}. However, increasing the power makes the function "too peaky". In practice, an exponent value between 5 and 15 might be a good trade-off between the required shallowness of the optimization function and the precision of the results.

2.8. The optimization problem

As discussed in Section 2.4, the goal in this study is to find brain sources whose $\langle f_i \rangle$, f_{loc}, or f_{peak} is maximally correlated to a target variable z in all epochs of data. We also introduced the least squares optimization problem in Equation 9, which is simplified as the following:

$$\min_{\mathbf{w}} \sum_{n=1}^{n_e} \big(z_n - \beta f_{\text{src},n}(\mathbf{w})\big)^2 \tag{16}$$

with $f_{\text{src},n}(\mathbf{w}) = f_{\text{src}}\big(\mathbf{w}\mathbf{x}_n(t)\big)$.

Equation 16 follows the standard formulation of an ordinary linear regression. By vectorizing z_n and $f_{s,n}(\mathbf{w})$ of all epochs in $\mathbf{z}$ and $\boldsymbol{f}_s(\mathbf{w})$, respectively, β can be analytically computed as follows:

$$\beta = \big(\mathbf{f}_{\text{src}}(\mathbf{w})^\top\mathbf{f}_{\text{src}}(\mathbf{w})\big)\mathbf{f}_{\text{src}}(\mathbf{w})^\top\mathbf{z} \tag{17}$$

Using this β as a function of $\mathbf{w}$ the optimization problem in 16 can be solved using the Matlab® function *lsqnonlin*. Two technical considerations in using this function are:

1. It converges to a local minimum. The solutions of 50 runs of the function (with different initial values) were used to select the one with the best fit, i.e. the one with the smallest sum of residuals.
2. Both vectors $\mathbf{z}$ and $\mathbf{f}_{\text{src}}(\mathbf{w})$ were normalized after each iteration during the optimization.

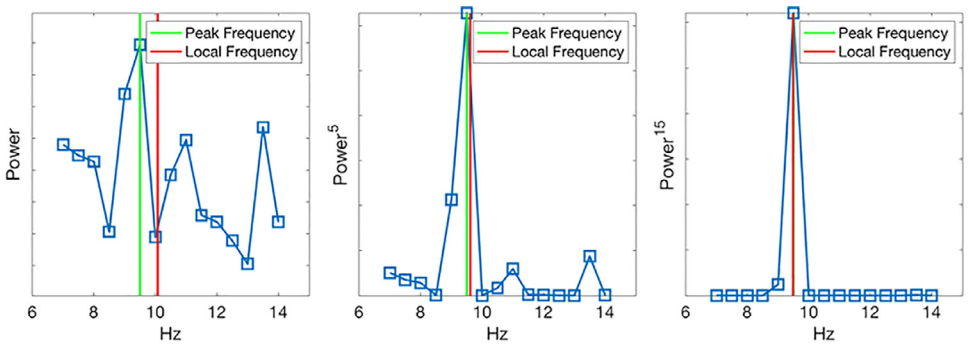

Fig. 2. Estimation of f_{loc} and f_{peak} using PS (left panel) and higher powers of bins of PS (middle panel exponent 5 and right panel exponent 15).

Finally, the spatial pattern of the source signal was obtained by multiplying the spatial filter with the data covariance matrix for IFD and with the real cross-spectral matrix for LFD and PFD (see e.g. Haufe et al. (2014b); Parra et al. (2005); Vidaurre et al. (2019b) for more details). The spatial location of the sources in the brain can be found using inverse modeling techniques such as eLORETA (Pascual-Marqui et al., 2011) or beamformers (Van Veen et al., 1997) applied on the computed spatial patterns.

Note that our decomposition methods return only one spatial filter, thus they only obtain the source whose frequency shift measure is maximally correlated with the experimental variable of interest. If one is interested in finding more than one source, a deflation method can be employed.

2.9. Simulations

2.9.1. Parameter description for artificially generated data

General parameter description The epoch length (or trial length) is a parameter of all three methods IFD, LFD, and PFD. Additionally, the signal-to-noise ratio has a direct impact on the performance of any source separation method. We performed our simulations with different values of epoch length and SNR to study how our methods perform with different parameter settings.

Also, the band in which the EEG data is generated might have an impact on the performance of all decomposition techniques. Therefore, we generated data in different frequency bands; delta (1-4 Hz), theta (4-8 Hz), alpha (8-13 Hz), beta (13-28 Hz), and gamma (40-70 Hz).

Finally, in the case of PFD, the impact of the exponent p was assessed by using four values of 5, 10, 12, and 15. This is a range covering diverse scenarios. For example, for noisy data where the power spectrum might present several peaks, a lower exponent might be advisable to avoid overfit to noise peaks. On the contrary, if data are clean, a higher exponent might provide more accurate results.

Parameter settings for different analyses

We studied the performance of our decomposition methods in detail for the alpha band, defined between 8 and 13 Hz. There we investigated the effect of different epoch lengths (namely 500 ms, 1000 ms, 2000 ms, and 3000 ms) and also different SNR values (0.1, 0.5, and 1).

IFD, LFD and PFD are, to the best of our knowledge, the first methods relating to the maximization of the correlation between the frequency fluctuations and a target variable. Therefore, we compared the results from our methods with a multivariate approach based on multiple linear regression using $\langle f_i \rangle$, f_{loc} and f_{peak} of each channel and trial as predictors. Additionally, we used the best correlation obtained in sensor space using Laplacian derivations. The comparison with a single best channel was included because this type of sensor-based analysis approach is usually employed in studies analyzing frequency shifts over time (see Mierau et al. (2017) for a review of studies). In these analyses, we are interested in the performance obtained with data generated in the alpha band at four different epoch lengths and three different SNR values.

Finally, in order to assess the impact of the operating frequency band on the performance of our decomposition methods, we restricted the epoch length to 2000 ms and the SNR to 0.5 and changed the frequency ranges in which EEG data was generated to delta, theta, alpha, beta, and gamma oscillations.

2.9.2. Recovery of ground truth patterns

Decomposition methods return a spatial filter that, as previously discussed, can be converted to a brain pattern. In order to analyze how similar the spatial pattern of the recovered source is to the ground truth pattern we estimated a "pattern recovery error" or RecErr that takes values between 0 (no error) and 1. The formula takes advantage of the scalar product between two vectors and can be defined as follows:

$$\text{RecErr} = 1 - \frac{|\boldsymbol{a}_o^\top \boldsymbol{a}_r|}{\|\boldsymbol{a}_o\| \cdot \|\boldsymbol{a}_r\|} \tag{18}$$

with $\boldsymbol{a}_o$ the original simulated pattern, $\boldsymbol{a}_r$ the pattern recovered by the corresponding decomposition method and $\|.\|$ the vector norm.

2.9.3. Artificially generated data description

Our proposed methods should find spatial filters whose frequency estimate of interest ($\langle f_i \rangle$, f_{loc} or f_{peak}) is maximally correlated to an experimental variable. To statistically test this goal we generated four different EEG sources. Their frequency and amplitude individually changed from trial to trial within the selected band and a total of 400 trials were generated. The trial length was a varying parameter (500 to 3000 ms), as discussed in Section 2.9.1. As an experimental variable, we selected the changing frequency of one of the four sources, thus the method should find the spatial filter related to this source.

To generate these artificial data, 40 EEG channels were fitted to the outermost layer of the standard Montreal Neurological Institute (MNI) head (Evans et al., 1994). The EEG forward solutions were obtained with a head model based on a three-compartment realistic volume conductor (Nolte and Dassios, 2005). The brain sources were defined as pseudo-random cortical dipoles. EEG oscillations were generated by band-pass filtering independent white noise in the frequency band of interest (a different one per trial and per source). In the case of the correlated source, the peak frequency of the source was also the target variable. A bandwidth of 2 Hz (1 Hz on each side of the peak frequency) was applied to generate the time series of the correlated source. As mentioned before, the target frequency changed every trial and the amplitude was modulated randomly. This target frequency was selected as an experimental variable, i.e. z_n in Equation 16, because its correlation to the source of interest is ideally one.

Background EEG noise was generated with 500 uncorrelated dipoles of random orientation and distribution on the cortex. The noise sources had $1/f$ type spectra. The SNR was calculated as the ratio between the mean variance across channels for the projected sources and the mean variance of additive noise (produced by all noise dipoles) in the center frequency of the brain source.

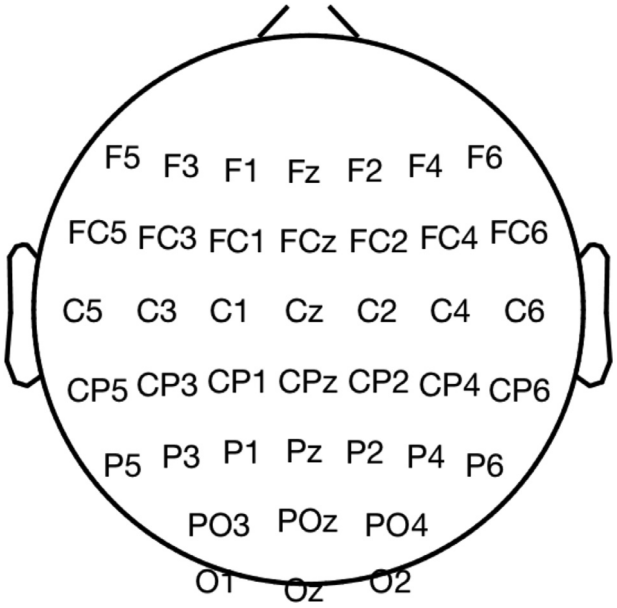

Fig. 3. Selected channels to analyse SSVEP data.

The sampling frequency of the simulation was 200 Hz.

In order to perform statistical analyses on simulation results, artificial data for each parameter combination were generated 200 times using random source locations and random peak frequencies for each trial and source.

2.10. SSVEP BCI data

We used data from a steady-state visual evoked potential (SSVEP) brain-computer interface (BCI) for assessing the performance of our proposed methods on real data. SSVEP data are a good choice for this study because the ground truth peak frequency is known (the flickering frequency at which the participant stares) and serves as a real test for all decomposition methods presented.

2.10.1. Data description

We used the publicly available dataset from (Iscan and Nikulin, 2018). It consists of data from 24 subjects who underwent an offline session where the participants were attending four different stimuli (circles) in distinct locations and flickering frequencies: 5.45 (up), 8.57 (down), 12 (right), and 15 (left) Hz. The participants performed a total of 100 trials, with 25 trials of each class. The sampling rate was originally 1000 Hz, but after bandpass filtering the data between 3 and 40 Hz, the data were downsampled to 200 Hz. EEG data were segmented using the stimuli markers that specify the start and end of the flickering. Four different epoch lengths were studied (500, 1000, 2000, and 3000 ms). 60 EEG channels were recorded with a reference electrode on the left mastoid. After removing electrodes on the most external positions, 41 channels were left for further analyses as presented in Fig. 3.

Data analysis was performed in MATLAB (2018b; The MathWorks, Natick, MA) using the BBCI toolbox (Blankertz et al., 2016), the Fieldtrip toolbox (Oostenveld et al., 2011), the EEGlab toolbox (Delorme and Makeig, 2004) and custom programmed software.

2.10.2. Data preprocessing

The preprocessing of the data included a dimensionality reduction step using Spatio-Spectral Decomposition (SSD, Haufe et al. (2014a); Nikulin et al. (2011); Vidaurre et al. (2021)) in the frequency band 5-17 Hz. The top ten SSD filters (ten times less than the number of trials) were selected based on their SNR, and then stacked in a matrix to build a multi-channel data matrix. IFD, LFD, and PFD were applied to this data matrix. In this way, the data in the SSD subspace were decomposed. Therefore, the computed mixing patterns of the decomposition methods should be projected back to the sensor space. Formally, if $\mathbf{p} \in \mathbb{R}^{10\times 1}$ is the mixing pattern in the SSD subspace, and $\mathbf{A}_{\text{ssd}} \in \mathbb{R}^{40\times 10}$ is the mixing matrix of the ten SSD components, the final spatial pattern of the extracted source on the sensor space is $\mathbf{a} = \mathbf{A}_{\text{ssd}}\mathbf{p}$.

2.11. Benchmark methods

In order to benchmark our results against conventional methods, we performed comparisons with multiple linear regression (MLR) and the best correlation result from Laplacian channels.

2.11.1. The best correlation from Laplacian channels

Although these are single-channel results, they are interesting because they are often reported in the literature (see e.g. Mierau et al. (2017)). To obtain the desired results, all channels were spatially filtered with a small Laplacian derivation (Sannelli et al., 2011). Those sensors that did not have enough neighboring channels were filtered with the available neighbors. Then, $\langle f_i \rangle$, f_{loc}, and f_{peak} were computed for each of the filtered channels, obtaining one value per epoch. These values were then correlated with the variable of interest and the result providing the highest correlation was selected for further comparisons.

2.11.2. Multiple linear regression (MLR)

MLR is a multivariate method often used to maximize the correlation between a dependent variable and multiple independent measures (Gasser et al., 1988; Iemi et al., 2022; Stephani et al., 2021; Thut et al., 2006; Zimmermann et al., 2010). This approach is often used to benchmark against novel multivariate approaches (see for example Dähne et al. (2014a)). Here, we computed instantaneous/local/peak frequencies of all the channels as regressors. The variable of interest (peak frequency of the generated trial) was used as a response variable. This way, a correlation value of the estimated target variable and the ground truth target variable was obtained.

Finally, it is worth noting that, in this case, the weights obtained from applying multiple linear regression cannot be interpreted in terms of topographies (sources) because they do not follow the generative model of the EEG/MEG signals.

2.12. Statistical analyses

Statistical analyses were performed in R (Team-R-Core, 2018) using beta regression models with *betareg* (Zeileis et al., 2016), version 3.1-4. Beta regression models were used since the dependent variables varied primarily between 0 and 1, and these models assume that the data follow a beta distribution. The performance of each decomposition method was evaluated with correlation values and recovery errors, such that higher correlation values and lower recovery error values were indicative of better performance. To compare the performance of different decomposition methods, correlation and recovery error were each modeled separately as functions of the *method* and *epoch length*. This procedure was carried out for each level of SNR. SNR was not included as a factor because we were not interested in its interaction with the other variables. It is known from real data analyses that better results are expected when the quality of data improves. Moreover, in real applications, the SNR value is usually not known.

Additionally, the performance of different frequency bands was analyzed using a fixed SNR and epoch length, with factors *method* and *band*.

The correlations obtained with MLR and the best Laplacian derivation using different frequency estimates ($\langle f_i \rangle$, f_{loc}, f_{peak}) were also investigated. Thus, beta regression models were built separately for MLR and Laplancian derivations. As before, the procedure was carried out for each level of SNR, using factors *method* and *epoch length*.

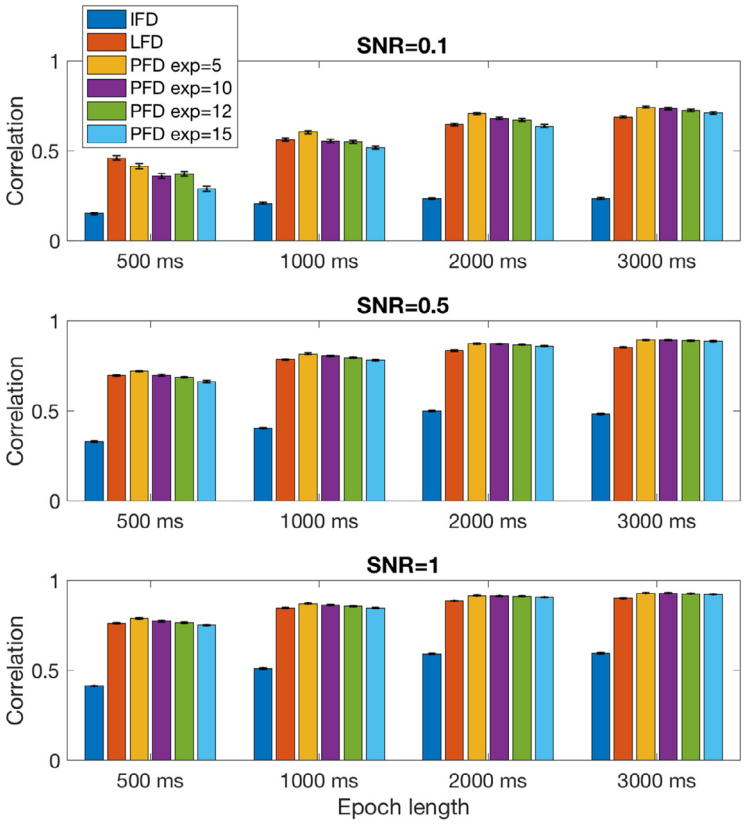

Fig. 4. Bar plot of averaged correlation values over 200 repetitions for each of the three methods (IFD, LFD, PFD) with different parameters. On the top, results with SNR=0.1 are visible, the middle panel displays results for SNR=0.5, and the bottom panel for SNR=1. The four groups of bars were obtained with different epoch lengths (500, 1000, 2000 and 3000 ms). Finally, the last four bars of each group are related to PFD with four different exponents (5, 10, 12, and 15, respectively). The error bars indicate the standard error of the mean.

Finally, for each frequency shift estimate, the corresponding decomposition method, MLR and the best Laplacian derivation performances were compared between each other.

Differences in performance within the previously described beta models were quantified by the estimated marginal means of pair-wise differences between factor levels, using the R package *emmeans*. Estimated marginal means are group means adjusted for means of other factors in the model (Searle et al., 1980). The p-values were adjusted using Tukey's HSD (honestly significant difference) test (Tukey, 1949).

3. Results

3.1. Simulations in the alpha band

3.1.1. Correlation results with decomposition methods

Simulations were conducted for validating the performance of the three proposed methods, namely IFD, LFD, and PFD. In Fig. 4, the correlation strengths averaged over 200 repetitions for IFD, LFD, and PFD are depicted in bar plots for different parameter values, i.e. different epoch length and SNR values. IFD performed consistently worse than LFD and PFD for all parameter combinations. Additionally, correlation results improved with longer epochs and, as expected, with higher SNR.

In order to investigate whether any of the methods obtained significantly higher correlations than the others, we performed three beta regressions with factors *method* and *epoch length* (one for each SNR). The performance of PFD was averaged over all exponents to obtain a composite result. The interaction and the main effects were all significant in all tests (see Table C.1). Post-hoc analyses carried out with HSD, showed that IFD performed significantly worse than LFD and PFD for all epoch lengths and in all SNRs. IFD showed much lower correlation values, with differences compared to LFD and PFD ranging from 0.26 to 0.49 (see Table C.2). PFD and LFD were not found significantly different for SNR=0.1. Otherwise, PFD was significantly better than LFD. Differences in correlation between them were small, ranging from 0.012 to 0.031. The smallest differences were found for higher SNRs and longer epoch lengths.

Post-hoc analyses concerning the difference between epoch lengths within methods showed that the longer the epoch, the higher the correlation obtained, except for SNR=0.5 and epoch lengths 2000 ms and 3000 ms, where results were not significantly different. The difference in performance w.r.t. epoch length seems to be higher for IFD (see Table C.3). To summarize, IFD was the worst method and although PFD performed significantly better than LFD, their correlation values were very close to each other.

3.1.2. Accuracy of pattern recovery

All decomposition methods proposed in this study return a spatial filter from which the spatial patterns of the sources are computed and can be localized by source reconstruction methods. The simulated data allow for the comparison between the location of the recovered source and the ground truth. This comparison can be quantified in terms of the "pattern recovery error" defined in Equation 18. Averaged recovery errors over repetitions for all decomposition methods are depicted in the bar plots of Fig. 5.

The beta regression for SNR=0.1 showed significant interactions between factors (*method* and *epoch length*) and significant main effects, whereas the two beta regressions for SNR=0.5 and SNR=1 showed only significant main effects (see Table C.4). For all SNRs, post-hoc analyses showed that LFD and PFD recovered sources significantly better than IFD for all epoch lengths. Also, LFD was significantly better than PFD in all cases, but differences between them were 10 times smaller in comparison to those found against IFD (see Table C.5).

Considering differences in Recovery Errors across epoch lengths within a method, the higher the SNR the lower the differences in errors in different lengths. In fact, for SNR=1, the differences between epochs with different lengths are not significant or are rather very small (for 2000 ms vs 500 ms). Also, for SNR=0.5, differences between 1000, 2000, and 3000 ms are not significant for any of the decomposition methods.

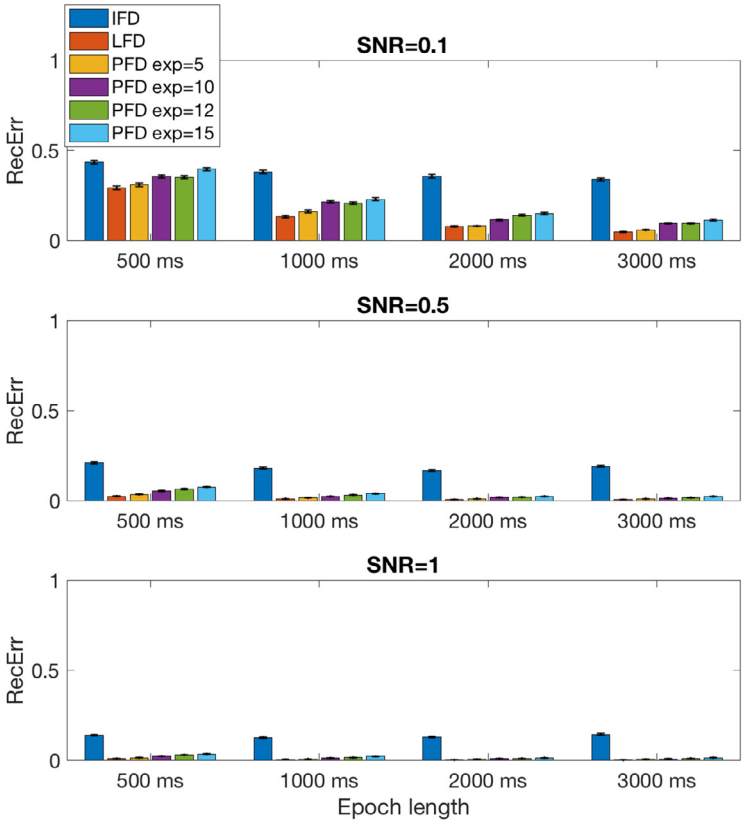

Fig. 5. Bar plot of averaged (over 200 repetitions) RecErr of IFD, LFD and PFD. The upper panel displays results with SNR=0.1, the middle panel with SNR=0.5, and the bottom panel with SNR=1. The four groups of bars were obtained with different epoch lengths (500, 1000, 2000 and 3000 ms).

Table 1
Average correlation values of benchmarking methods over 200 repetitions for each frequency shift measure, SNR and epoch length.

	SNR	MLR Corr.				Lap. Corr.			
		Epoch length(ms)				Epoch length(ms)			
		500	1000	2000	3000	500	1000	2000	3000
$\langle f_i \rangle$	0.1	0.35	0.39	0.44	0.45	0.15	0.19	0.23	0.24
	0.5	0.47	0.56	0.65	0.66	0.24	0.31	0.39	0.41
	1	0.53	0.63	0.72	0.74	0.29	0.38	0.46	0.49
f_{loc}	0.1	0.35	0.41	0.47	0.52	0.15	0.19	0.24	0.26
	0.5	0.48	0.60	0.69	0.73	0.25	0.33	0.40	0.44
	1	0.55	0.68	0.76	0.80	0.31	0.41	0.48	0.52
f_{peak}	0.1	0.34	0.39	0.41	0.43	0.14	0.17	0.21	0.23
	0.5	0.44	0.52	0.61	0.64	0.23	0.29	0.69	0.38
	1	0.51	0.61	0.68	0.72	0.28	0.36	0.43	0.46

However, with a low SNR of 0.1, longer epochs obtain significantly better results, with 500 ms being not long enough to provide acceptable results in comparison to 1000, 2000, and 3000 ms (see Table C.6).

The recovered topographies (spatial patterns) of the sources extracted with the three proposed methods in an exemplar simulation are depicted in Fig. 6. This figure shows that LFD and PFD with different exponents could accurately recover the original source. IFD displayed much higher RecErr than LFD and PFD, but the recovered topography resembled well the original one. However, it is not possible to recover patterns of sources with the coefficients obtained from applying MLR. Thus, the difference between the original source and the regression coefficient was remarkably high. Therefore, researchers performing this type of analysis need to bear in mind that it is not possible to interpret regression coefficients in terms of brain sources.

3.1.3. Correlation results with benchmark methods

Table 1 shows the average correlation values over 200 repetitions that resulted from applying MLR (columns 3 to 6) and Laplacian filters (columns 7 to 10) to $\langle f_i \rangle$, f_{loc} and f_{peak}. As expected MLR values are greater than the best Laplacian derivation results. Also, f_{loc} appears to obtain better results than $\langle f_i \rangle$ and f_{peak}.

Three beta regressions were performed to compare results from MLR using different frequency shift estimates, one for each SNR. The interaction between factors and the main effects were all significant (see Table C.7). HSD post-hoc analyses showed that MLR with f_{loc} achieved significantly better correlation values than with f_{peak} and $\langle f_i \rangle$. Finally, $\langle f_i \rangle$ was found significantly better than f_{peak} as well. However, differences between frequency shift estimates were not big, ranging from approximately 0.09 to 0.02 (see Table C.8). As before, longer epochs implied better correlation results, with differences getting smaller with increasing epoch lengths (see Table C.9).

The same procedure was applied to the correlation obtained with the best Laplacian derivation. Beta regression models on all SNRs returned significant main effects, but no significant interactions (see Table C10). Post-hoc analyses showed that f_{loc} correlations were always significantly better than f_{peak} results. Furthermore, f_{loc} correlations were only not significantly different than $\langle f_i \rangle$ for SNR=1.0. Finally, no significant differences were found between $\langle f_i \rangle$ and f_{peak}. Comparing results over different epoch lengths for the same frequency estimates revealed that the correlations at longer epochs were always significantly stronger than at shorter ones, except for 2000 and 3000 ms, where differences were not significant (see Table C.11 and C.12).

3.1.4. Comparison of decomposition methods with multiple linear regression and best Laplacian derivation

The comparison between decomposition and benchmark methods was performed with beta regression models, one for each SNR and for each frequency shift measure ($\langle f_i \rangle$, f_{loc} or f_{peak}). After fixing the SNR and the frequency measure, the factors were two: *method* (MLR, best Laplacian channel, and the corresponding decomposition method) and *epoch length*. The results of interest for each frequency estimate were

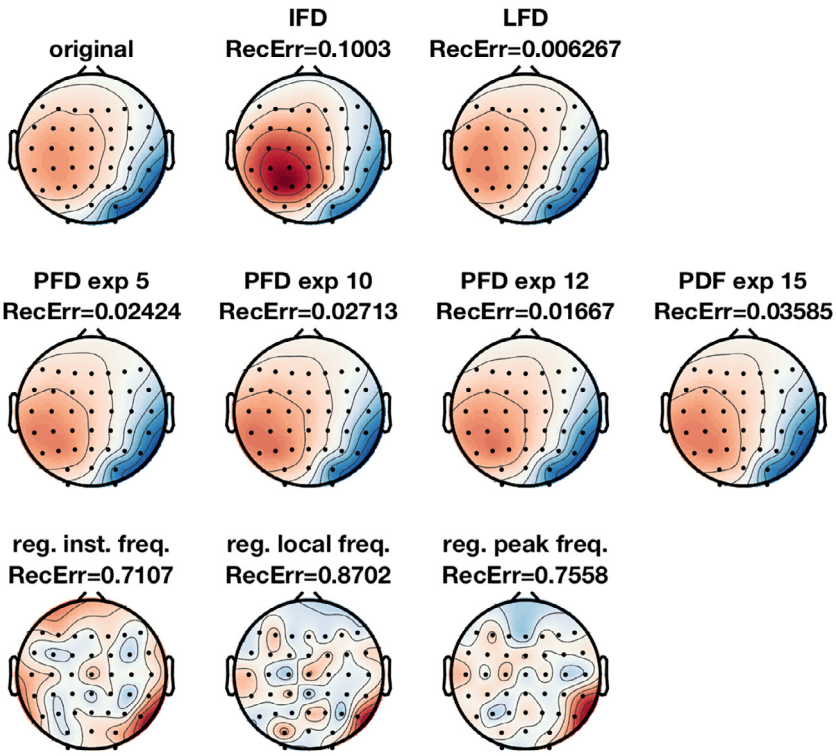

Fig. 6. Top: left, topography of the original generated source; middle, topography recovered with IFD and the corresponding RecErr; right, topography recovered with LFD and corresponding RecErr. Middle: topographies recovered with PFD and different exponents. RecErr of each of them is also displayed. Bottom: regression coefficients depicted over the scalp. Although they do not correspond to sources, we computed RecErr to highlight their deviation from the original pattern.

concerning whether one method was significantly better than the rest in each of the epoch lengths.

Results indicated for $\langle f_i \rangle$ that main effects were significant for all SNRs, whereas the interaction was significant only for SNR=0.5 (see Table C.13). Post-hoc analyses showed that MLR obtained better correlation values than IFD and the best Laplacian channel for all SNRs, with a difference of around 0.2 between MLR and the rest. Also, IFD and best Laplacian were not significantly different for SNR=0.1 regardless of the epoch length. However, for SNR=0.5 and SNR=1, IFD results were significantly better than those obtained with the best Laplacian derivation, in a range between 0.06 and 0.09 approximately (see Table C.14, first nine rows).

Conversely, in the case of f_{loc}, interactions and main effects were all significant (see rows 10 to 18 of Table C.13). Regarding post-hoc comparisons, LFD was significantly better than MLR and the best Laplacian channel on f_{loc} in all epoch lengths and for all SNRs, with differences in correlation around 0.2 to 0.15 and 0.5 to 0.3 respectively. Also, MLR was significantly better than Laplacian with differences ranging between 0.25 and 0.19 approximately (see rows 10 to 18 of Table C.14).

Concerning f_{peak}, interactions and main effects were all significant (see last nine rows of Table C.13). PFD was significantly better than MLR (differences between 0.33 and 0.19 in correlation) and the best Laplacian channel (differences ranging between 0.57 and 0.37) for all epoch lengths and SNRs. MLR was also significantly better than the best Laplacian derivation (between 0.24 and 0.17 difference in correlation).

3.2. Simulations in different frequency bands

It is also of relevance to analyze how the performance of our decomposition methods is affected by the frequency range of the analyzed brain oscillations. To this end, we averaged the performance obtained by each method in different bands, after fixing SNR to 0.5 and epoch length to 2000 ms. Fig. 7 shows averaged correlation values (top) and recovery errors (bottom) of the three decomposition methods for each band. The value of PFD is an averaged composite of all exponents.

Two beta regression models with factors *frequency band* and *method* were performed, one for correlation values and another one for recovery errors. All main effects and both interactions were significant (see Tables C.15 and C.18). Fig. 7 shows that IFD does not perform as well as LFD and PFD in terms of correlation values (differences between 0.52 and 0.31, see rows 1 to 10 of Table C.16) or recovery errors (differences between 0.21 and 0.17, see Table C.19), just as expected from the previous analysis in the alpha band in Section 3.1.1. The differences between LFD and PFD were much lower (from 0.07 in the delta band to 0.043 in alpha for correlation values and 0.031 in recovery errors, see Table C16 and C19, respectively).

Concerning the performance of IFD in different bands, IFD in the delta band performs worse than the rest, with differences in correlation values between 0.21 and 0.29. Although some differences between the rest of the frequency bands are significant, they perform fairly similarly, with differences in correlation values ranging from 0.07 to 0.01 (see first 10 rows of Table C.17). Considering recovery errors, these are not so different from each other in comparison to the correlation values. Differences between the delta band and the other frequency bands are between 0.08 and 0.02 (the latter is not significant). Differences among the other frequency bands are also small and oscillate between 0.06 and 0 (see first ten rows of Table C20).

Similar results were found for the performance of LFD, i.e., larger differences were found comparing correlation values of the delta band with correlation values of the other frequency bands (ranging between 0.28 and 0.21) than among the other frequency bands (0.077 to 0.01), see rows 11 to 20 in Table C.17. Comparable differences in recovery errors were also present for LFD (differences between 0.082 and 0.018 for delta band versus the other frequency bands and between 0.064 and 0.001 among the rest of frequency bands), see Table C.20.

Finally, PFD showed smaller differences between bands, but again, the difference in correlation values was larger comparing the delta band

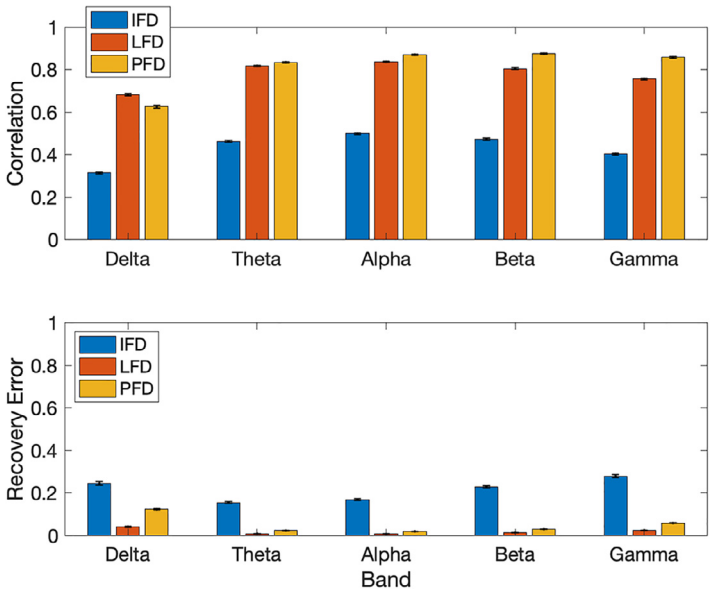

Fig. 7. Upper panel: bar plot of averaged correlation values over 200 repetitions for each of the three methods (IFD, LFD, PFD) in each frequency band. Bottom panel: bar plot of averaged recovery errors over 200 repetitions for each of the three methods (IFD, LFD, PFD) in each frequency band.

with the rest of the frequency bands (0.11 to 0.088) than among the other frequency bands (0.028 to 0.003), see last 10 rows of Table C.17. Concerning recovery errors, differences between the delta band vs. the other frequency bands were again larger (0.082 to 0.018) than among the other frequency bands (0.064 to 0.001), see Table C.20.

3.3. Real data from SSVEP BCI

We applied the three proposed methods to EEG data recorded from participants performing an SSVEP BCI experiment. As aforementioned, these data were selected because the ground truth is ideally the frequency the participant stares at. Thus, it is the same type of data as the one used in simulations, where the correlation of frequency shifts along the experiment and the frequency used as the target variable must be very high. The final goal of this analysis was to find out whether the obtained sources had a plausible topography with respect to the nature of the visual BCI experiment.

The results of simulations with SNR=0.5 showed that for short time windows (500 and 1000 ms) an exponent of 5 was good and for longer ones an exponent between 10 and 15 would give good results (see Fig. 4). Thus, to obtain correlation values with PFD in these experiments we selected exponent 5 for 500 and 1000 ms epochs and exponent 12 for 2000 and 3000 ms.

3.3.1. Correlation values of decomposition methods

Average correlation values over participants for each decomposition method are summarized in Table 2 together with the standard error of the mean (sem). As observed in the simulations, IFD correlations were much lower than LFD and PFD. In this case, PFD returned higher correlation values than LFD.

Beta regression models comparing methods and epoch lengths showed that the main effects and the interaction were all significant (see Table C.21). The post-hoc analyses revealed that IFD was significantly worse than LFD and PFD for all epoch lengths, with differences in correlation results ranging from 0.14 to 0.33 and 0.44 to 0.17, respectively. LFD was significantly worse than PFD, with differences (0.1 to 0.04) decreasing as the epoch length increased (see Table C.22). Regarding epoch lengths, the longer the epoch, the better the correlation, except for 2000 and 3000 ms, where differences were not significantly different. Also, differences for PFD and LFD seem smaller than for IFD (see Table C.23).

Table 2
Average correlation values over subjects and standard error of the mean.

Method	Epoch length	Correlation value
	(ms)	(mean ± sem)
IFD	500	0.48±0.02
	1000	0.61±0.02
	2000	0.73±0.02
	3000	0.76±0.02
LFD	500	0.75±0.02
	1000	0.86±0.02
	2000	0.91±0.02
	3000	0.92±0.01
PFD	500	0.78±0.02
	1000	0.88±0.02
	2000	0.95±0.01
	3000	0.96±0.01

3.3.2. Comparison of decomposition against benchmark methods

The scatter plots of correlations obtained with decomposition methods versus MLR and best Laplacian derivation for each frequency shift estimate (columns) and each epoch length (rows) are depicted in Fig. 8. Each participant is represented as an orange circle (the best Laplacian derivation vs. decomposition method) or a blue cross (MLR vs. decomposition method). Similar to the simulations, LFD and PFD obtained better results than MLR and the best Laplacian channel, whereas IFD was worse than MLR but better than the best Laplacian derivation for all epoch lengths tested. Analogously to the simulations, LFD and PFD obtained better results than MLR and the best Laplacian channel, whereas IFD was worse than MLR but better than the best Laplacian derivation for all epoch lengths tested.

Three beta regression models for each of the frequency shift estimates were performed with factors *method* (the corresponding decomposition methods, MLR, and best Laplacian) and *epoch length*. All interactions and main effects were significant (see Table C.24). Post-hoc analyses showed that Laplacian derivations were significantly worse than MLR (differences in correlation between 0.52 and 0.33) and IFD (range of differences between 0.36 and 0.24) for all epoch lengths. Otherwise, MLR was significantly better than IFD (differences between 0.16 and 0.09), see Table C.25.

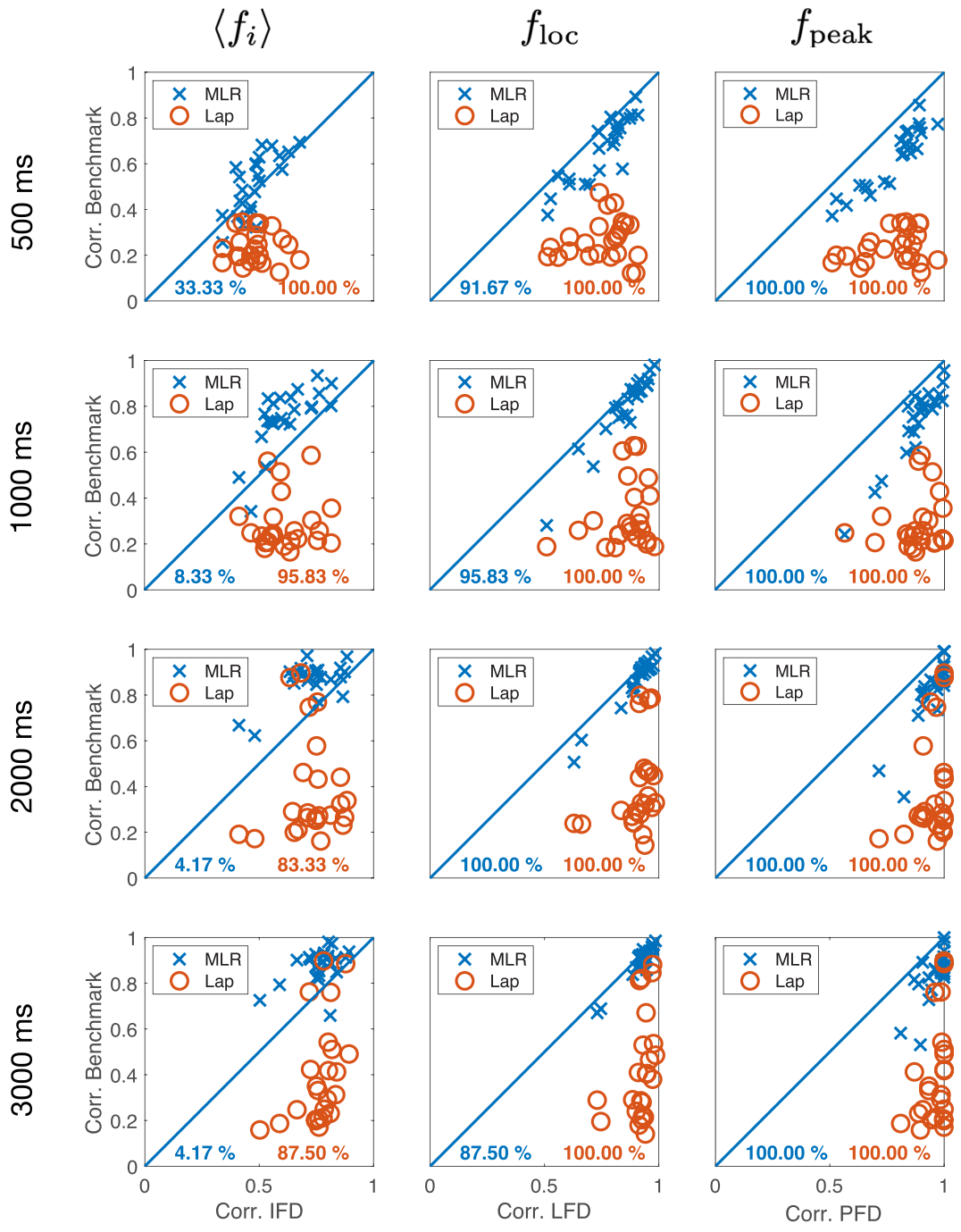

Fig. 8. Scatter plot of correlation results of real SSVEP data. Each row depicts results for one epoch length, from 500 ms (upper row) to 3000 ms (bottom row). Each column is obtained with a different frequency shift estimate. Column 1: IFD vs. benchmark methods computed using $\langle f_i \rangle$. Column 2: LFD vs. benchmark methods computed using f_{loc}. Column 3: PFD vs. benchmark methods estimated using f_{peak}. In each plot, the x-axis represents results delivered by the corresponding decomposition method and the y-axis results of MLR (blue crosses) and best Laplacian derivation (orange circles) using the corresponding frequency shift estimate. Each point on the scatter plot represents the correlation results of one subject. All values below the diagonal indicate that the correlation of the corresponding decomposition method was higher than the correlation of the corresponding benchmark method for that specific subject.

With respect to local and peak frequencies, their corresponding decomposition methods were significantly better than MLR and the best Laplacian derivation. Differences between LFD and MLR ranged between 0.06 and 0.03, and between PFD and MLR they were in the interval 0.22 to 0.11. The differences against Laplacian derivations were between 0.6 and 0.4 for local frequency and between 0.75 and 0.44 for peak frequency. Also, MLR was significantly better than the best Laplacian in both cases (0.56 to 0.36 for local frequency and 0.53 to 0.33 for peak frequency, see Table C25).

3.3.3. *Spatial pattern dissimilarities*

Finally, grand averages of EEG patterns for each decomposition method were computed over all participants. Before averaging, a global sign of each topography was adjusted across the subjects to avoid polarity cancellation. Results are depicted on the top panel of Fig. 9, together with some PFD topographies of three exemplar subjects on the bottom panel. The cortical sources corresponding to each of the patterns were also computed. The inverse modeling was performed with eLORETA (Pascual-Marqui et al., 2011) using the S-Meth Toolbox (Nolte, 2023).

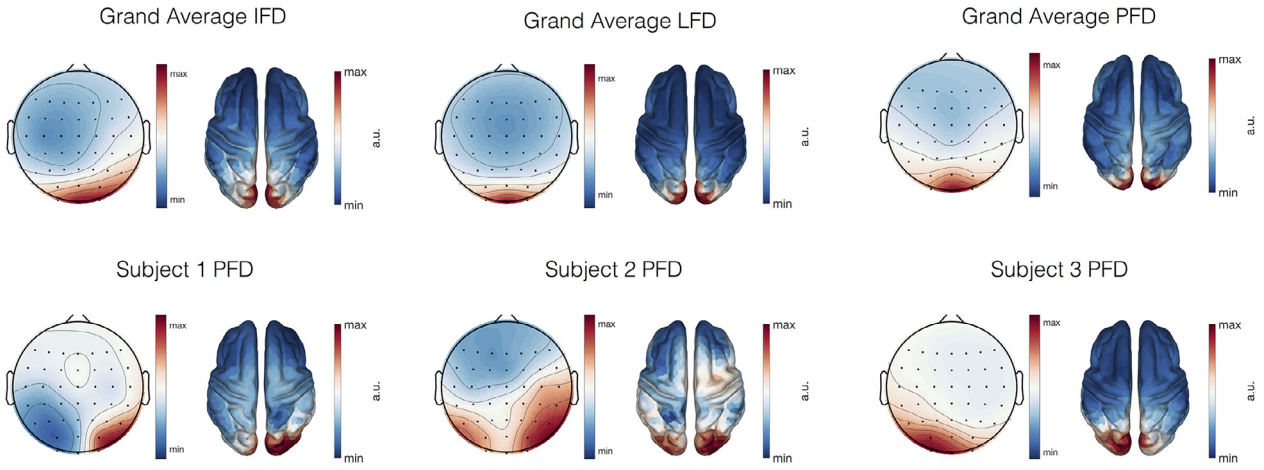

Fig. 9. Top: average across subjects spatial patterns obtained with IFD, LFD and PFD. On their right, the corresponding source localization using eLORETA also for IFD, LFD, and PFD. Bottom: subject-specific spatial patterns of PFD and their corresponding source localizations.

The active sources displayed in all sub-figures were primarily localized over the occipital cortex.

Additionally, we computed the mutual dissimilarity of the spatial patterns among all participants using Equation 18. Here the main idea was to see the consistency of the topographies across participants. It ranged between 0.55 and 0.85. This in turn indicates a high variability of neural sources between subjects.

As expected by the experimental paradigm, all subjects show occipital patterns. However, dissimilarities between them exist, demonstrating that our decomposition methods can be used to study individual differences between subjects.

4. Discussion

Three methods were presented to find spatial projections for multichannel sensor data (i.e. the latent source) leading to maximum (anti-)correlation between its instantaneous frequency, local frequency, or peak frequency and an experimental variable. All methods are based on the minimization of the mean squared error. Our simulations showed that the introduced algorithms are capable of recovering sources with changing frequencies even with very low SNR and that they can recover physiologically meaningful sources in real EEG recordings. Below, we discuss different aspects relating to their application.

4.1. Which decomposition method performs better?

IFD, LFD, and PFD allow the recovery of source components whose frequency shift estimates are maximally correlated to an external variable of interest. To the best of our knowledge, this is not possible with any other method. The neural sources corresponding to spatial patterns can be then reconstructed using inverse models such as eLORETA (Pascual-Marqui et al., 2011) or beamformers (Van Veen et al., 1997).

The most important result with respect to the developed algorithms and their ability to maximize correlations is related to the differences between IFD and the two methods LFD and PFD, which are applied to data in the frequency domain. IFD obtained significantly worse results for all parameters tested (SNR and epoch length) and also worse results regarding the recovery of the generated source of interest (see Fig. 4). This means that not only the correlation was not high (0.5 to 0.27 less correlation than LFD and PFD), but also the pattern recovery error (see Fig. 5) was much larger than for LFD and PFD (up to 0.27 more), meaning that the recovered source does not resemble the original source as accurately as PFD and LFD.

IFD appears more sensitive to noise than LFD and PFD. This may relate to the calculation of instantaneous frequency as a local derivative of phase. Despite the applied averaging, the derivative amplifies the noise present in the frequency band of interest leading to phase jumps (Freeman, 2004). This in turn leads to worse results in comparison to the spectral counterparts, which are defined directly in the frequency domain. Furthermore, because the definition of f_i is related to the multiplication of two numbers, (see the numerator in Equation 10), there is no guaranty that the final result lies in the frequency band of interest.

The statistical analyses on simulation results showed that PFD exhibits a slight advantage over LFD (up to 0.03 difference in correlation). These small values suggest that both LFD and PFD are competitive methods to find sources related to frequency shifts over time.

Concerning the accuracy of recovering mixing patterns of sources, Fig. 5 shows that LFD and PFD could accurately recover the ground-truth generated pattern, even though three other sources with frequency-fluctuating oscillatory components were also present in the simulated data. Although differences between PFD and LFD were significant, both methods returned low recovery errors, especially for higher SNR values and longer windows. This was, however, not the case for IFD, which performed worse in all settings, similar to the results of the correlation values. The results also show that under low SNR conditions epochs of preferably 1000 ms or longer should be used.

4.2. Instantaneous, local, or peak frequency estimates in sensor space, which one obtains better correlation values?

Despite the presence of noise in all EEG channels, previous studies investigating peak frequency or instantaneous frequency have been carried out primarily in sensor space (Mierau et al., 2017). To take such approaches into account, here we also performed some simulations to benchmark our newly developed methods against sensor-space approaches. Regarding correlations of frequency estimates using Laplacian derivations with a variable of interest, f_{loc} offered the highest accuracy, and $\langle f_i \rangle$ was slightly better than f_{peak}. We hypothesize that f_{loc} is a more stable estimate against noise present in channel data: on the one hand, its formula is not based on derivatives like the formula of f_i, which in low signal to noise ratio situations might mainly reflect noise, and on the other hand, its definition is not related to peaks, whose location might be unstable in the presence of noise. Yet, these results were inferior compared to LFD and PFD decomposition methods.

Concerning MLR results, f_{loc} delivered the best correlation values. On the other hand, $\langle f_i \rangle$ obtained quite similar results to f_{peak}, especially for low SNRs. Although MLR is a multivariate method, when it is applied to measures involving non-linear transformations such as f_{peak}, f_{loc}, or $\langle f_i \rangle$, it cannot separate noise from the signal of interest (Dähne et al., 2014b). Thus MLR is as sensitive to channel noise as Laplacian channel based results. As before, f_{peak} and $\langle f_i \rangle$ seem to be

more sensitive to noise, and thus results obtained with them are worse than those of f_{loc}.

Hence, and in agreement with the mathematical discussion on the relationship between f_{loc} and $\langle f_i \rangle$ presented in Section 2.4, we recommend choosing f_{loc} over $\langle f_i \rangle$ if averages can be performed over data windows or epochs.

4.3. Are decomposition methods better than regression or channel-based models?

Decomposition methods are in general preferable in comparison to single channel or regression approaches (Dähne et al., 2014b; Haufe et al., 2014a; Idaji et al., 2020; Nikulin et al., 2011). First, they are able to separate source information from noise and improve the interpretability of the estimates. In contrast, single-channel methods and regression models based on channel estimates involving non-linear operations suffer from the mixing of noise and signals from multiple oscillatory sources (Vidaurre et al., 2019b).

Second, the mixture of signal and noise poses a serious problem also in relation to the interpretation of results and the location of their cortical origin. Although spatial filters such as Laplacian derivations can reduce the effect of noise from remote sources, they might also remove oscillations that contribute to the sources of interest.

Regarding the first point (interpretability of the results), the correlation results obtained for MLR of f_{loc} and f_{peak} were significantly lower than correlations obtained with LFD and PFD. LFD and PFD correlation results were also significantly better than results obtained using the Laplacian derivation with the highest correlation. These single-channel results were also significantly worse than MLR analyses.

Considering the second aspect (source unmixing), the spatial filters found by PFD and LFD reflect sources but were also able to remove part of the noise contribution from the 500 noise dipoles included in the simulation. Thus, they were able to separate signal and noise and improve the interpretation of the obtained results. However, this was not the case for IFD which, as previously discussed, is too sensitive to the effect of noise on phase estimation and could not obtain better correlation values compared to MLR.

Another advantage of decomposition methods, such as the ones presented in this study, is their ability to provide patterns or data topographies of cortical sources that are related to the research hypothesis. For example, in Fig. 6 one can see that LFD and PFD can accurately recover the original source, whereas the weights of the different MLR procedures do not reflect the cortical origin of the source of interest. Such patterns facilitate the following reconstruction of the neural data since they reflect a small set of contributing neuronal elements.

It should be remarked that inverse source localization techniques are often used to extract brain sources. However, these methods typically require an accurate forward model and generate a large amount of data which in turn leads to the application of statistical methods compensating multiple comparisons. Finally, source localization techniques do not typically incorporate information about the research variable of interest which is an advantage of LFD and PFD approaches.

4.4. Performance of decomposition methods in different frequency bands

Frequency shifts related to experimental variables might be of interest in any of the frequency bands in which EEG/MEG oscillations are categorized. Thus, we also studied the performance of our decomposition methods over different frequency bands.

As discussed for results in the alpha band, IFD performed worse than LFD and PFD for all bands, and also achieved worse recovery errors.

Concerning the frequency domain methods, results show that LFD and PFD perform similarly in the theta, alpha, beta, and gamma bands, with differences in performance that are in some cases significant, but small. Furthermore, in the delta band, the average correlation is still high (above 0.6) for both methods. The difference observed between the delta band and the other frequency bands is probably related to the length of the segment employed, which in the case of delta contains less cycles of the oscillation of interest due to its low frequency rate.

4.5. Application to real data

The averaged topographies obtained from the application of decomposition methods on SSVEP BCI data were related to activities in the occipital areas, a result that is in agreement with previous studies (Jorajuría et al., 2020; 2021; Srinivasan et al., 2006). Although we used eLORETA for source localization, any other inverse modeling technique could be utilized (Michel et al., 2004).

Note that the patterns can also be studied in a subject-dependent manner, as visible in Fig. 9. Although these patterns generally indicate the location of neural sources in occipito-parietal cortex, one can also observe subject-specific spatial configurations. In fact, the dissimilarity between patterns was in some cases relatively high, thus indicating that the analysis in sensor space across subjects might lead to inconclusive results due to a selective mixture of neural sources at each electrode (Vidaurre et al., 2019b). Therefore, in addition to conventional sensor space analysis, we recommend running PFD or LFD for more consistent results across participants when using frequency shift estimations.

In fact, the EEG data projected onto the spatial filters obtained by decomposition methods provide time courses that directly represent source activity. These time courses can be used to investigate temporal dynamics of the corresponding sources *without the use of inverse modeling*. For instance, when investigating the dependency of behavioral performance with some experimental variable or the generation of evoked responses depending on the frequency of pre-stimulus alpha oscillations, one can use the projected data obtained with PFD or LFD. As shown in our simulations this approach should lead to better detection of dependencies compared to sensor space approaches.

We also believe that PFD and LFD can be used for tracking changes in alpha peak frequency induced by transcranial alternating current stimulation (tACS) (Gundlach et al., 2020). In these studies. one can investigate whether and how the peak frequency of alpha oscillations is entrained by tACS with a varying stimulation frequency. Due to the excellent performance of PFD/LFD even with very low SNR one is more likely to detect subtle changes in the dynamics of ongoing alpha oscillations compared to conventional sensor-space analysis.

4.6. Limitations and future work

Although the proposed methods were extensively tested with simulations and real data, there are still limitations linked to them, which we elaborate upon in the following.

Similar to almost all data decomposition methods, the performance of the presented algorithms depends on the data quality, i.e., SNR. Our simulations show that LFD and PFD perform well even in a very low SNR value of 0.1, and that as the SNR increases, the methods perform more reliably.

Another limitation of the proposed methods is related to the temporal and frequency resolution, i.e. the length of the trials or the sliding windows. While IFD obtains one instantaneous frequency value per time sample, LFD and PFD obtain one frequency estimate per data window in which the frequency transforms are applied. In real data, the operating frequency of the oscillations is not known a priori. In general, the temporal and frequency resolution defined by the window length impose a limitation on how well the methods can capture frequency changes. In experimental paradigms where the external variable changes faster than the temporal resolution of the decomposition methods, a sliding window technique may be useful. The above-mentioned means that, if one is interested in changes occurring in a narrow band, one should be aware that those variations should be slow in time, because the high frequency resolution required to study effects in narrow bands, is inevitably linked to a low temporal resolution (Bruns, 2004).

We would like to remark that, as shown in Bruns (2004), Fourier-, Hilbert- and wavelet-based signal analyses are all formally equivalent and none of them provides an advantage over the rest, meaning that IFD does not contain more information than LFD and PFD, provided that all of them are applied using similar sets of parameters. Yet, as our results show, LFD and PFD allow a better extraction of the corresponding neuronal sources.

Finally, peak frequencies can be affected by aperiodic $1/f$ noise, especially in situations where the SNR is very low. In that case, disentangling the effect of the background noise on the peak frequency can be achieved by estimating the slope of the $1/f$ part of spectra in sequential time windows (for instance with the FOOOF algorithm, (Donoghue et al., 2020)) and then relating it to the changes in the frequency of oscillations. This would allow ensuring that the changes in the frequencies are not driven primarily by the changes in the aperiodic part of spectra. For instance in a recent study (Cesnaite et al., 2023) it was shown that aging affects peak frequency and $1/f$ noise differently thus providing evidence for the distinct neuronal mechanisms relating to both phenomena.

Considering possible future works that are beyond the scope of this paper, we think that an interesting extension might be adapting our decomposition methods to a discriminative framework where the external variable of interest can only take two discrete values.

5. Conclusions

Understanding which brain activities hold the key to comprehend brain function when analyzing experiments in cognitive neuroscience is a challenge. So far, typically sensor space analyses are applied and unsupervised models are used. Here, we have contributed novel approaches for source space analysis, that are supervised, i.e. they directly relate to labels.

Specifically, three different source separation methods to find oscillatory sources whose frequency fluctuates in maximal (anti-) correlation to an experimental variable of interest are proposed. We explained the mathematical relation between all estimates and showed that both methods based on measures computed in the frequency domain (i.e. local frequency LFD and peak frequency PFD) provide significantly better results than the method based on instantaneous frequency, IFD. Also, LFD and PFD provide significantly better results than multivariate linear regression. Furthermore, our source separation methods, unlike MLR, provide spatial filters that can be related to networks of sources whose frequency fluctuations are correlated to the experimental variable of interest. Results on real EEG data further show the ability of LFD and PFD to obtain neurophysiologically plausible sources.

In summary, we consider our proposed source separation methods helpful tools to broadly investigate and gain better insights on perceptual, motor and cognitive processes in the brain.

Data and Code Availability Statement

The authors used a publicly available dataset that was freely shared by Iscan and Nikulin (2018). Parts of code might be shared upon request. Iscan, Z., Nikulin, V., 2018. Steady state visual evoked potential (SSVEP) based brain-computer interface (BCI) performance under different perturbations. PLOS ONE 13 (1), 1-17.

Declaration of Competing Interest

The authors declare that they have no known competing financial interests or personal relationships that could have appeared to influence the work reported in this paper.

Credit authorship contribution statement

C. Vidaurre: Conceptualization, Methodology, Software, Validation, Formal analysis, Writing – original draft, Project administration, Funding acquisition, Writing – review & editing. **K. Gurunandan:** Methodology, Software, Validation, Formal analysis, Writing – original draft. **M. Jamshidi Idaji:** Validation, Writing – original draft, Writing – review & editing, Visualization. **G. Nolte:** Methodology, Software, Validation, Formal analysis, Writing – review & editing. **M. Gómez:** Writing – review & editing. **A. Villringer:** Resources, Writing – review & editing. **K.-R. Müller:** Resources, Writing – review & editing. **V.V. Nikulin:** Conceptualization, Supervision, Formal analysis, Methodology, Validation, Writing – review & editing.

Acknowledgements

C.V. was supported by the Spanish Ministry of Economy with Grant RyC 2014-15671, Spanish Ministry of Research and Innovation PID2020-118829RB-100, H2020-FETPROACT-EIC-2018-2020 Grant MAIA-951910, Diputacion Foral de Gipuzkoa Brain2Move project, Diputacion Foral de Gipuzkoa Neurocog Project, and Ikerbasque (Basque Foundation for Science). K.G. was supported by the Basque Government postdoctoral grant POS-2021-1-0007. G.N. was partially funded by the German Research Foundation (DFG, SFB936 Z3 and TRR169, B4). K.-R.M. work was supported by German Ministry for Education and Research (BMBF) under Grants 01IS14013A-E, 01GQ1115 and 01GQ0850; by the Institute of Information & Communications Technology Planning & Evaluation (IITP) grants funded by the Korea government (MSIT) (No. 2019-0-00079, Artificial Intelligence Graduate School Program, Korea University and No. 2022-0-00984, Development of Artificial Intelligence Technology for Personalized Plug-and-Play Explanation and Verification of Explanation). Correspondence to CV, VN and KRM.

Appendix A. Derivation of the instantaneous frequency of a brain source

This appendix describes the mathematical derivations necessary to define f_i of one brain source according to the linear model of the EEG. If $s_a(t)$ is the analytical signal of $s(t)$ and we denote its argument as $\phi(t)$, $s_a(t)$ can be written as:

$$s_a(t) = |s_a(t)|e^{j\phi(t)} \tag{A.1}$$

and:

$$e^{j\phi(t)} = \frac{s_a(t)}{|s_a(t)|} \tag{A.2}$$

taking derivatives over time on the above equation:

$$\frac{d\phi(t)}{dt} j e^{j\phi(t)} = \frac{d}{dt}\frac{s_a(t)}{|s_a(t)|} \tag{A.3}$$

Substituting Equation A.2 in Equation A.3 and rearranging:

$$\frac{d\phi(t)}{dt} = \frac{|s_a(t)|}{j s_a(t)} \frac{d}{dt}\frac{s_a(t)}{|s_a(t)|} = \frac{\frac{ds_a(t)}{dt}|s_a(t)| - s_a(t)\frac{d|s_a(t)|}{dt}}{j s_a(t)|s_a(t)|} \tag{A.4}$$

On the other hand:

$$\frac{d|s_a(t)|}{dt} = \frac{d\sqrt{s_a(t)s_a^*(t)}}{dt} = \frac{\frac{ds_a(t)}{dt}s_a^*(t) + s_a(t)\frac{ds_a^*(t)}{dt}}{2|s_a(t)|} \tag{A.5}$$

where * denotes complex conjugate. Substituting Equation A.5 on Equation A.4 we arrive to:

$$\frac{d\phi(t)}{dt} = \frac{\frac{ds_a(t)}{dt}s_a^*(t) - s_a(t)\frac{ds_a^*(t)}{dt}}{2j|s_a(t)|^2} = \Im\left\{\frac{\frac{ds_a(t)}{dt}s_a^*(t)}{|s_a(t)|^2}\right\} \tag{A.6}$$

Thus, $f_i(t)$ in Equation 6 can be written as:

$$f_i(t) = \frac{1}{2\pi}\Im\left\{\frac{\frac{ds_a(t)}{dt}s_a^*(t)}{|s_a(t)|^2}\right\} \tag{A.7}$$

Writing the previous equation in terms of the backward model in Equation 3, we arrive at Equation 10.

Appendix B. Derivation of the local frequency of a brain source

This appendix describes how f_{loc} of a brain source can be mathematically derived according to the linear model of the EEG. Recall here that the spectrum of the analytic signal is 0 for negative frequencies, it coincides with the value of the real signal at $f = 0$ and it is twice the value otherwise. For a band-limited signal between $f_1 \neq 0$ and $f_2 \neq 0$, Equation 8 can be rewritten as the following:

$$f_{\text{loc}} = \frac{\int_{f_1}^{f_2} f|S_a(f)|^2 df}{\int_{f_1}^{f_2} |S_a(f)|^2 df} = \frac{\int_{f_1}^{f_2} f|2S(f)|^2 df}{\int_{f_1}^{f_2} |2S(f)|^2 df} = \frac{\int_{f_1}^{f_2} f|S(f)|^2 df}{\int_{f_1}^{f_2} |S(f)|^2 df} \tag{B.1}$$

where $S(f)$ is the spectrum of the real-valued signal. In practice, the signal was divided into overlapping time segments, with each segment windowed using a Hann function. Its corresponding spectrum was determined using fast Fourier transform (FFT). Finally, the squared magnitude of the spectrum was computed. Taking into account that all signals are sampled, the f_{loc} formula is then:

$$f_{\text{loc}}(n) = \frac{\sum_{f=f_1}^{f_2} f S(f,n) S(f,n)^*}{\sum_{f=f_1}^{f_2} S(f,n) S^*(f,n)} \tag{B.2}$$

where $S(f,n)$ denotes the FFT of the n-th epoch (windowed by a Hann function) at frequency bin f. Then, employing the backward model in Equation 3, we can rewrite the square magnitude of the spectrum of the n-th epoch of a brain source signal $s(t) = \mathbf{w}^\top \mathbf{x}(t)$ as:

$$|S(n,f)|^2 = S(f,n)S(f,n)^* = \mathbf{w}^\top \Re\{\boldsymbol{\mathcal{X}}(f,n)\boldsymbol{\mathcal{X}}^{\text{H}}(f,n)\}\mathbf{w} \tag{B.3}$$

where $\boldsymbol{\mathcal{X}}(f,n)$ is the spectrum of sensor signals $\mathbf{x}(t)$ (windowed by the Hann function) at frequency bin f and centered in window n, and $\boldsymbol{\mathcal{X}}^{\text{H}}(f,n)$ is its conjugate transpose (or Hermitian transpose). Taking the real part of the product of Fourier transforms in Equation B.3 is enough, because as $\boldsymbol{\mathcal{X}}(f,n)\boldsymbol{\mathcal{X}}^{\text{H}}(f,n)$ is hermitian, the final result after multiplying with $\boldsymbol{w}^\top$ and $\boldsymbol{w}$ is a real value.

Substituting equation B.3 in Equation B.2 and given that the weights are not frequency nor epoch dependent, we obtain:

$$f_{\text{loc}}(n,\mathbf{w}) = \frac{\sum_{f=f_1}^{f_2} f \mathbf{w}^\top \Re\{\boldsymbol{\mathcal{X}}(f,n)\boldsymbol{\mathcal{X}}^{\text{H}}(f,n)\}\mathbf{w}}{\sum_{f=f_1}^{f_2} \mathbf{w}^\top \Re\{\boldsymbol{\mathcal{X}}(f,n)\boldsymbol{\mathcal{X}}^{\text{H}}(f,n)\}\mathbf{w}} \tag{B.4}$$

$$= \frac{\sum_{f=f_1}^{f_2} \mathbf{w}^\top f \Re\{\boldsymbol{\mathcal{X}}(f,n)\boldsymbol{\mathcal{X}}^{\text{H}}(f,n)\}\mathbf{w}}{\sum_{f=f_1}^{f_2} \mathbf{w}^\top \Re\{\boldsymbol{\mathcal{X}}(f,n)\boldsymbol{\mathcal{X}}^{\text{H}}(f,n)\}\mathbf{w}} \tag{B.5}$$

$$= \frac{\mathbf{w}^\top \Big(\sum_{f=f_1}^{f_2} f \Re\{\boldsymbol{\mathcal{X}}(f,n)\boldsymbol{\mathcal{X}}^{\text{H}}(f,n)\} \Big)\mathbf{w}}{\mathbf{w}^\top \Big(\sum_{f=f_1}^{f_2} \Re\{\boldsymbol{\mathcal{X}}(f,n)\boldsymbol{\mathcal{X}}^{\text{H}}(f,n)\} \Big)\mathbf{w}} \tag{B.6}$$

which is the same as Equation 14.

Appendix C. Results of statistical analyses performed

Performance of the different methods was operationalised as correlations and recovery errors, and these performance measures were modeled using beta regressions, and the pairwise differences between methods were quantified using estimated marginal means. Beta regression models were used since recovery error values lie in the interval [0,1] and in practice, the correlation values were primarily positive. To account for the few negative correlation values, the vectors were rescaled from [-1,1] to [0,1] (see Douma and Weedon (2019)) for the purposes of modeling, and then the estimated marginal means were back-transformed to the original scale. To keep analyses and results consistent and comparable between the different variables, we followed this same procedure for all variables.

C.1. *Statistical tests of IFD, LFD and PFD with factors* method *and* epoch length

Table C.1
Interaction and main effects for correlation values obtained with decomposition methods in each SNR. Methods are IFD, LFD and PFD.

SNR	Factor	Df	Chisq	Pr(>Chisq)
0.1	Method	2	1897.82	<0.001 ***
	Epoch	3	453.36	<0.001 ***
	Method:Epoch	6	192.50	<0.001 ***
0.5	Method	2	5904.03	< 0.001 ***
	Epoch	3	968.81	< 0.001 ***
	Method:Epoch	6	187.18	<0.001 ***
1.0	Method	2	6970.40	<0.001 ***
	Epoch	3	1239.50	< 0.001 ***
	Method:Epoch	6	148.94	< 0.001 ***

Signif. codes: <0.001 '***', < 0.01 '**', <0.05 '*', >0.05 n.s.

Table C.2
Estimated marginal means of correlation difference between methods at different epochs.

SNR	Contrast	500 ms	1000 ms	2000 ms	3000 ms
0.1	IFD - LFD	-0.435***	-0.398***	-0.366***	-0.350***
	IFD - PFD	-0.437***	-0.399***	-0.367***	-0.351***
	LFD - PFD	-0.001 n.s.	-0.001, n.s.	-0.001, n.s.	-0.001, n.s.
0.5	IFD - LFD	-0.465***	-0.391***	-0.325***	-0.315***
	IFD - PFD	-0.496***	-0.415***	-0.344***	-0.333***
	LFD - PFD	-0.031***	-0.024***	-0.019***	-0.018***
1.0	IFD - LFD	-0.431***	-0.341***	-0.277***	-0.264***
	IFD - PFD	-0.454***	-0.357***	-0.29***	-0.276***
	LFD - PFD	-0.023***	-0.017***	-0.013***	-0.012***

Signif. codes: <0.001 '***', < 0.01 '**', <0.05 '*', >0.05 n.s.

Table C.3
Estimated marginal means of correlation difference between epoch lengths within different decomposition methods.

SNR	Contrast	IFD	LFD	PFD
0.1	500 ms. - 1000 ms.	-0.141***	-0.104***	-0.103***
	500 ms. - 2000 ms.	-0.238***	-0.169***	-0.168***
	500 ms. - 3000 ms.	-0.281***	-0.196***	-0.195***
	1000 ms. - 2000 ms.	-0.097***	-0.065***	-0.065***
	1000 ms.- 3000 ms.	-0.141***	-0.092***	-0.092***
	2000 ms.- 3000 ms.	-0.043*	-0.027*	-0.027*
0.5	500 ms. - 1000 ms.	-0.143***	-0.069***	-0.062***
	500 ms. - 2000 ms.	-0.259***	-0.118***	-0.106***
	500 ms. - 3000 ms.	-0.275***	-0.125***	-0.112***
	1000 ms. - 2000 ms.	-0.115***	-0.049***	-0.044***
	1000 ms. - 3000 ms.	-0.132***	-0.056***	-0.05***
	2000 ms. - 3000 ms.	-0.016, n.s.	-0.007, n.s.	-0.006, n.s.
1.0	500 ms. - 1000 ms.	-0.143***	-0.069***	-0.062***
	500 ms. - 2000 ms.	-0.259***	-0.118***	-0.106***
	500 ms. - 3000 ms.	-0.275***	-0.125***	-0.112***
	1000 ms. - 2000 ms.	-0.115***	-0.049***	-0.044***
	1000 ms. - 3000 ms.	-0.132***	-0.056***	-0.05***

Signif. codes: <0.001 '***', < 0.01 '**', <0.05 '*', >0.05 n.s.

Table C.4
Interaction and main effects for recovery errors of decomposition methods for different SNR.

SNR	Factor	Df	Chisq	Pr(>Chisq)
0.1	Method	2	572.733	<0.001 ***
	Epoch	3	329.739	<0.001 ***
	Method:Epoch	6	30.337	<0.001 ***
0.5	Method	2	1473.080	<0.001 ***
	Epoch	3	45.245	<0.001 ***
	Method:Epoch	6	10.060	0.1222 n.s.
1.0	Method	2	1544.8262	<0.001 ***
	Epoch	3	8.6975	0.0336 *
	Method:Epoch	6	8.4801	0.2050 n.s.

Signif. codes: <0.001 '***', < 0.01 '**', <0.05 '*', >0.05 n.s.

Table C.5
Estimated marginal means of errors obtained with decomposition methods at different epochs.

SNR	Contrast	500 ms	1000 ms	2000 ms	3000 ms
0.1	IFD - LFD	0.234***	0.262***	0.270***	0.274***
	IFD - PFD	0.205***	0.231***	0.239***	0.243***
	LFD - PFD	-0.028*	-0.031*	-0.031*	-0.032*
0.5	IFD - LFD	0.185***	0.186***	0.186***	0.186***
	IFD - PFD	0.167***	0.168***	0.168***	0.168***
	LFD - PFD	-0.018**	-0.018**	-0.018**	-0.018**
1.0	IFD - LFD	0.133***	0.134***	0.134***	0.134***
	IFD - PFD	0.123***	0.123***	0.123***	0.123***
	LFD - PFD	-0.01*	-0.01*	-0.01*	-0.01*

Signif. codes: <0.001 '***', < 0.01 '**', <0.05 '*', >0.05 n.s.

Table C.6
Estimated marginal means of recovery error difference between epoch lengths within different decomposition methods.

SNR	Contrast	IFD	LFD	PFD
0.1	500 ms. - 1000 ms.	0.122***	0.15***	0.147***
	500 ms. - 2000 ms.	0.174***	0.21***	0.207***
	500 ms. - 3000 ms.	0.204***	0.244***	0.241***
	1000 ms. - 2000 ms.	0.052***	0.06***	0.06***
	1000 ms. - 3000 ms.	0.082***	0.094***	0.094***
	2000 ms. - 3000 ms.	0.03, n.s.	0.034, n.s.	0.034, n.s.
0.5	500 ms. - 1000 ms.	0.025***	0.026***	0.026***
	500 ms. - 2000 ms.	0.038***	0.039***	0.039***
	500 ms. - 3000 ms.	0.03***	0.032***	0.032***
	1000 ms. - 2000 ms.	0.013, n.s.	0.013, n.s.	0.013, n.s.
	1000 ms. - 3000 ms.	0.005, n.s.	0.005, n.s.	0.005, n.s.
	2000 ms. - 3000 ms.	-0.007, n.s.	-0.008, n.s.	-0.008, n.s.
1.0	500 ms. - 1000 ms.	0.01, n.s.	0.01, n.s.	0.01, n.s.
	500 ms. - 2000 ms.	0.011*	0.012*	0.012*
	500 ms. - 3000 ms.	0.006, n.s.	0.006, n.s.	0.006, n.s.
	1000 ms. - 2000 ms.	0.001, n.s.	0.001, n.s.	0.001, n.s.
	1000 ms. - 3000 ms.	-0.004, n.s.	-0.004, n.s.	-0.004, n.s.
	2000 ms. - 3000 ms.	-0.005, n.s.	-0.005, n.s.	-0.005, n.s.

Signif. codes: <0.001 '***', < 0.01 '**', <0.05 '*', >0.05 n.s.

C.2. Statistical tests of MLR with factors frequency shift estimate *and* epoch length *for different SNR*

Table C.7
Interaction and main effects for correlation values obtained with MLR and different frequency estimates ($\langle f_i \rangle$, f_{loc}, f_{peak}).

SNR	Factor	Df	Chisq	Pr
0.1	Fr. Est.	2	215.915	< 0.001 ***
	Epoch	3	936.2833	< 0.001 ***
	Fr. Est.:Epoch	6	99.292	< 0.001 ***
0.5	Fr. Est.	2	275.442	< 0.001 ***
	Epoch	3	2233.399	< 0.001 ***
	Fr. Est.:Epoch	6	64.395	<0.001 ***
1.0	Fr. Est.	2	298.268	< 0.001 ***
	Epoch	3	2558.223	< 0.001 ***
	Fr. Est.:Epoch	6	55.894	< 0.001 ***

Signif. codes: <0.001 '***', < 0.01 '**', <0.05 '*', >0.05 n.s.

Table C.8
Estimated marginal means of correlations obtained with MLR and different frequency shift estimates.

SNR	Contrast	500 ms	1000 ms	2000 ms	3000 ms
0.1	$\langle f_i \rangle - f_{\text{loc}}$	-0.038***	-0.036***	-0.035***	-0.033***
	$\langle f_i \rangle - f_{\text{peak}}$	0.02***	0.019***	0.018***	0.018***
	$f_{\text{loc}} - f_{\text{peak}}$	0.058***	0.056***	0.053***	0.051***
0.5	$\langle f_i \rangle - f_{\text{loc}}$	-0.051***	-0.044***	-0.037***	-0.034***
	$\langle f_i \rangle - f_{\text{peak}}$	0.039***	0.034***	0.029***	0.027***
	$f_{\text{loc}} - f_{\text{peak}}$	0.091***	0.079***	0.066***	0.061***
1.0	$\langle f_i \rangle - f_{\text{loc}}$	-0.058***	-0.047***	-0.038***	-0.035***
	$\langle f_i \rangle - f_{\text{peak}}$	0.034***	0.028***	0.023***	0.021***
	$f_{\text{loc}} - f_{\text{peak}}$	0.092***	0.076***	0.061***	0.055***

Signif. codes: <0.001 '***', < 0.01 '**', <0.05 '*', >0.05 n.s.

Table C.9
Estimated marginal means of correlation difference between epoch lengths within different frequency shift estimates for MLR.

SNR	Contrast	$\langle f_i \rangle$	f_{loc}	f_{peak}
0.1	500 ms. - 1000 ms.	-0.041***	-0.039***	-0.041***
	500 ms. - 2000 ms.	-0.094***	-0.091***	-0.096***
	500 ms. - 3000 ms.	-0.122***	-0.117***	-0.124***
	1000 ms. - 2000 ms.	-0.054***	-0.052***	-0.055***
	1000 ms. - 3000 ms.	-0.081***	-0.078***	-0.082***
	2000 ms. - 3000 ms.	-0.027***	-0.026***	-0.028***
0.5	500 ms. - 1000 ms.	-0.102***	-0.095***	-0.107***
	500 ms. - 2000 ms.	-0.192***	-0.178***	-0.202***
	500 ms. - 3000 ms.	-0.225***	-0.208***	-0.238***
	1000 ms. - 2000 ms.	-0.09***	-0.083***	-0.095***
	1000 ms. - 3000 ms.	-0.123***	-0.113***	-0.131***
	2000 ms. - 3000 ms.	-0.033***	-0.03***	-0.035***
1.0	500 ms. - 1000 ms.	-0.112***	-0.101***	-0.118***
	500 ms. - 2000 ms.	-0.197***	-0.177***	-0.208***
	500 ms. - 3000 ms.	-0.226***	-0.203***	-0.24***
	1000 ms. - 2000 ms.	-0.085***	-0.075***	-0.09***
	1000 ms. - 3000 ms.	-0.115***	-0.102***	-0.122***
	2000 ms. - 3000 ms.	-0.03***	-0.026***	-0.032***

Signif. codes: <0.001 '***', < 0.01 '**', <0.05 '*', >0.05 n.s.

Table C.12
Estimated marginal means of correlation difference between epoch lengths within different frequency shift estimates for the best Laplacian derivation.

SNR	Contrast	$\langle f_i \rangle$	f_{loc}	f_{peak}
0.1	500 ms. - 1000 ms.	-0.042***	-0.042***	-0.042***
	500 ms. - 2000 ms.	-0.088***	-0.088***	-0.089***
	500 ms. - 3000 ms.	-0.11***	-0.109***	-0.111***
	1000 ms. - 2000 ms.	-0.046***	-0.046***	-0.047***
	1000 ms. - 3000 ms.	-0.068***	-0.068***	-0.068***
	2000 ms. - 3000 ms.	-0.022, n.s.	-0.022, n.s.	-0.022, n.s.
0.5	500 ms. - 1000 ms.	-0.083***	-0.082***	-0.085***
	500 ms. - 2000 ms.	-0.165***	-0.161***	-0.167***
	500 ms. - 3000 ms.	-0.196***	-0.193***	-0.2***
	1000 ms. - 2000 ms.	-0.081***	-0.079***	-0.083***
	1000 ms. - 3000 ms.	-0.113***	-0.11***	-0.115***
	2000 ms. - 3000 ms.	-0.032, n.s.	-0.031, n.s.	-0.033, n.s.
1.0	500 ms. - 1000 ms.	-0.1***	-0.098***	-0.102***
	500 ms. - 2000 ms.	-0.186***	-0.181***	-0.19***
	500 ms. - 3000 ms.	-0.22***	-0.213***	-0.225***
	1000 ms. - 2000 ms.	-0.086***	-0.083***	-0.088***
	1000 ms. - 3000 ms.	-0.12***	-0.116***	-0.123***
	2000 ms. - 3000 ms.	-0.034, n.s.	-0.033, n.s.	-0.035, n.s.

Signif. codes: <0.001 '***', < 0.01 '**', <0.05 '*', >0.05 n.s.

C.3. Statistical tests of best Laplacian channel with factors frequency shift estimate *and* epoch length *for each SNR*

Table C.10
Interaction and main effects for correlation values and different frequency estimates used for the best Laplacian derivation and different SNR.

SNR	Factor	Df	Chisq	Pr(>Chisq)
0.1	Fr. Est.	2	11.5909	0.003 **
	Fr. Est.	3	150.9316	<0.001 ***
	Method:Fr. Est.h	6	2.4612	0.872780 n.s.
0.5	Fr. Est.	2	15.8600	<0.001 ***
	Fr. Est.	3	227.5349	<0.001 ***
	Method:Fr. Est.	6	1.7247	0.9432 n.s.
1.0	Fr. Est.	2	19.0568	<0.001 ***
	Epoch	3	257.2585	<0.001 ***
	Method:Fr. Est.	6	1.9902	0.9206 n.s.

Signif. codes: <0.001 '***', < 0.01 '**', <0.05 '*', >0.05 n.s.

Table C.11
Estimated marginal means of correlations obtained with the best Laplacian derivation and different frequency shift estimates.

SNR	Contrast	500 ms	1000 ms	2000 ms	3000 ms
0.1	$\langle f_i \rangle - f_{\text{loc}}$	-0.01, n.s.	-0.009, n.s.	-0.009, n.s.	-0.009, n.s.
	$\langle f_i \rangle - f_{\text{peak}}$	0.019, n.s.	0.019, n.s.	0.019, n.s.	0.019, n.s.
	$f_{\text{loc}} - f_{\text{peak}}$	0.029**	0.028**	0.028**	0.028**
0.5	$\langle f_i \rangle - f_{\text{loc}}$	-0.028, n.s.	-0.027, n.s.	-0.025, n.s.	-0.024, n.s.
	$\langle f_i \rangle - f_{\text{peak}}$	0.025, n.s.	0.024, n.s.	0.022, n.s.	0.021, n.s.
	$f_{\text{loc}} - f_{\text{peak}}$	0.053***	0.05***	0.047***	0.046***
1.0	$\langle f_i \rangle - f_{\text{loc}}$	-0.036*	-0.034*	-0.031*	-0.029*
	$\langle f_i \rangle - f_{\text{peak}}$	0.026, n.s.	0.024, n.s.	0.022, n.s.	0.021, n.s.
	$f_{\text{loc}} - f_{\text{peak}}$	0.062***	0.058***	0.053***	0.05***

Signif. codes: <0.001 '***', < 0.01 '**', <0.05 '*', >0.05 n.s.

C.4. Comparison between decomposition methods, MLR and the best Laplacian Derivation for each frequency shift estimate

Table C.13
Interaction and main effects for correlation values obtained using different frequency shift estimates and applied to all decomposition methods, MLR and best Laplacian derivation.

SNR	Fr. Est.	Factors	Df	Chisq	Pr(>Chisq)
$\langle f_i \rangle$	0.1	Method	2	1159.255	< 0.001 ***
		Epoch	3	202.755	< 0.001 ***
		Method:Epoch	6	6.979	<0.3228 n.s.
	0.5	Method	2	798.122	< 0.0011 ***
		Epoch	3	536.548	< 0.001 ***
		Method:Epoch	6	14.448	0.025 *
	1.0	Method	2	694.669	< 0.001 ***
		Epoch	3	642.231	< 0.001 ***
		Method:Epoch	6	10.632	0.1004 n.s.
f_{loc}	0.1	Method	2	1735.8471	< 0.001 ***
		Epoch	3	325.459	< 0.001 ***
		Method:Epoch	6	52.114	< 0.001 ***
	0.5	Method	2	2402.695	< 0.001 ***
		Epoch	3	620.913	< 0.001 ***
		Method:Epoch	6	28.821	< 0.001 ***
	1.0	Method	2	2193.283	< 0.001 ***
		Epoch	3	643.576	< 0.001 ***
		Method:Epoch	6	19.245	0.004 **
f_{peak}	0.1	Method	2	2337.949	< 0.001 ***
		Epoch	3	470.13	< 0.001 ***
		Method:Epoch	6	393.27	< 0.001 ***
	0.5	Method	2	3682.15	< 0.001 ***
		Epoch	3	627.04	< 0.001 ***
		Method:Epoch	6	100.981	< 0.001 ***
	1.0	Method	2	3412.693	< 0.001 ***
		Epoch	3	606.259	< 0.001 ***
		Method:Epoch	6	48.832	< 0.001 ***

Signif. codes: <0.001 '***', < 0.01 '**', <0.05 '*', >0.05 n.s.

Table C.14
Estimated marginal means of correlations obtained with different frequency shift estimates and SNRs, comparison between decomposition method, MLR and best Laplacian derivation.

Fr. Est.	SNR	contrast	500	1000	2000	3000
$\langle f_i \rangle$	0.1	MLR - Lap	0.197***	0.192***	0.186***	0.185***
		MLR - IFD	0.201***	0.196***	0.19***	0.189***
		IFD - Lap	-0.004, n.s.	-0.004, n.s.	-0.004, n.s.	-0.004, n.s.
	0.5	MLR - Lap	0.243***	0.225***	0.201***	0.198***
		MLR - IFD	0.174***	0.16***	0.141***	0.14***
		IFD - Lap	0.069***	0.065***	0.059***	0.058***
	1.0	MLR - Lap	0.245***	0.217***	0.188***	0.182***
		MLR - IFD	0.149***	0.13***	0.112***	0.108***
		IFD - Lap	0.096***	0.086***	0.076***	0.074***
f_{loc}	0.1	MLR - Lap	0.224***	0.215***	0.204***	0.196***
		MLR - LFD	-0.192***	-0.179***	-0.164***	-0.155***
		LFD - Lap	0.417***	0.394***	0.368***	0.351***
	0.5	MLR - Lap	0.269***	0.238***	0.209***	0.195***
		MLR - LFD	-0.224***	-0.185***	-0.155***	-0.141***
		LFD - Lap	0.493***	0.422***	0.364***	0.336***
	1.0	MLR - Lap	0.266***	0.225***	0.192***	0.177***
		MLR - LFD	-0.206***	-0.161***	-0.131***	-0.118***
		LFD - Lap	0.473***	0.386***	0.323***	0.295***
f_{peak}	0.1	MLR - Lap	0.199***	0.191***	0.181***	0.176***
		MLR - PFD	-0.255***	-0.235***	-0.215***	-0.206***
		PFD - Lap	0.454***	0.425***	0.397***	0.381***
	0.5	MLR - Lap	0.236***	0.216***	0.193***	0.183***
		MLR - PFD	-0.337***	-0.288***	-0.243***	-0.225***
		PFD - Lap	0.573***	0.504***	0.436***	0.408***
	1.0	MLR - Lap	0.242***	0.214***	0.188***	0.176***
		MLR - PFD	-0.309***	-0.254***	-0.211***	-0.193***
		PFD - Lap	0.551***	0.469***	0.398***	0.369***

Signif. codes: <0.001 '***', < 0.01 '**', <0.05 '*', >0.05 n.s.

C.5. Statistical tests comparing different frequency bands for different decomposition methods at fixed epoch length and SNR

Table C.15
Interaction and main effects for correlation values in different frequency bands. Methods are IFD, LFD and PFD.

	Df	Chisq	Pr(>Chisq)
Method	2	5698.74	< 0.001 ***
Band	4	997.74	< 0.001 ***
Method:Band	8	408.29	< 0.001 ***

Signif. codes: <0.001 '***', < 0.01 '**', <0.05 '*', >0.05 n.s.

Table C.16
Estimated marginal means of correlation values obtained with decomposition methods at different bands.

Contrast	Band	EMM
IFD - LFD	delta	-0.455***
	theta	-0.342***
	alpha	-0.312***
	beta	-0.318***
	gamma	-0.354***
IFD - PFD	delta	-0.528***
	theta	-0.39***
	alpha	-0.355***
	beta	-0.361***
	gamma	-0.404***
LFD - PFD	delta	-0.072***
	theta	-0.048***
	alpha	-0.043***
	beta	-0.044***
	gamma	-0.05***

Signif. codes: <0.001 '***', < 0.01 '**', <0.05 '*', >0.05 n.s.

Table C.17
Estimated marginal means of correlation values obtained with decomposition methods at different bands.

Method	Contrast	EMM
IFD	delta - theta	-0.234***
	delta - alpha	-0.288***
	delta - beta	-0.279***
	delta - gamma	-0.211***
	theta - alpha	-0.054***
	theta - beta	-0.044**
	theta - gamma	0.023, n.s.
	alpha - beta	0.01, n.s.
	alpha - gamma	0.077***
	beta - gamma	0.067***
LFD	delta - theta	-0.121***
	delta - alpha	-0.145***
	delta - beta	-0.141***
	delta - gamma	-0.11***
	theta - alpha	-0.024***
	theta - beta	-0.02**
	theta - gamma	0.011, n.s.
	alpha - beta	0.004, n.s.
	alpha - gamma	0.035***
	beta - gamma	0.031***
PFD	delta - theta	-0.096***
	delta - alpha	-0.115***
	delta - beta	-0.112***
	delta - gamma	-0.088***
	theta - alpha	-0.019***
	theta - beta	-0.016**
	theta - gamma	0.008, n.s.
	alpha - beta	0.003, n.s.
	alpha - gamma	0.028***
	beta - gamma	0.024***

Signif. codes: <0.001 '***', < 0.01 '**', <0.05 '*', >0.05 n.s.

Table C.18
Interaction and main effects for error values in different frequency bands. Methods are IFD, LFD and PFD.

Factor	Df	Chisq	Pr(>Chisq)
Method	2	1687.79	< 0.001 ***
Band	4	211.63	< 0.001 ***
Method:Band	8	102.24	< 0.001 ***

Signif. codes: <0.001 '***', < 0.01 '**', <0.05 '*', >0.05 n.s.

Table C.19
Estimated marginal means of error values obtained with decomposition methods at different bands.

Contrast	Band	EMM
IFD - LFD	delta	0.207***
	theta	0.212***
	alpha	0.212***
	beta	0.21***
	gamma	0.208***
IFD - PFD	delta	0.176***
	theta	0.18***
	alpha	0.18***
	beta	0.179***
	gamma	0.177***
LFD - PFD	delta	-0.031***
	theta	-0.031***
	alpha	-0.031***
	beta	-0.031***
	gamma	-0.031***

Signif. codes: <0.001 '***', < 0.01 '**', <0.05 '*', >0.05 n.s.

Table C.20
Estimated marginal means of errors obtained with decomposition methods at different bands.

Method	Contrast	EMM
IFD	delta - theta	0.078***
	delta - alpha	0.077***
	delta - beta	0.05***
	delta - gamma	0.017, n.s.
	theta - alpha	0, n.s.
	theta - beta	-0.028***
	theta - gamma	-0.061***
	alpha - beta	-0.027***
	alpha - gamma	-0.06***
	beta - gamma	-0.033***
LFD	delta - theta	0.082***
	delta - alpha	0.082***
	delta - beta	0.053***
	delta - gamma	0.018, n.s.
	theta - alpha	-0.001, n.s.
	theta - beta	-0.029***
	theta - gamma	-0.064***
	alpha - beta	-0.028***
	alpha - gamma	-0.063***
	beta - gamma	-0.035***
PFD	delta -theta	0.082***
	delta - alpha	0.081***
	delta - beta	0.053***
	delta - gamma	0.018, n.s.
	theta - alpha	-0.001, n.s.
	theta - beta	-0.029***
	theta - gamma	-0.064***
	alpha - beta	-0.028***
	alpha - gamma	-0.063***
	beta - gamma	-0.035***

Signif. codes: <0.001 '***', < 0.01 '**', <0.05 '*', >0.05 n.s.

C.6. Statistical tests of decomposition methods IFD, LFD and PFD applied to real SSVEP data

Table C.21
Interaction and main effects for correlation values obtained using different decomposition methods applied to real SSVEP data. The method here means IFD, LFD or PFD.

Factor	Df	Chisq	Pr(>Chisq)
Method	2	387.388	<0.001 ***
Epoch	3	218.410	<0.001 ***
Method:Epoch	6	38.277	<0.001 ***

Signif. codes: <0.001 '***', < 0.01 '**', <0.05 '*', >0.05 n.s.

Table C.22
Estimated marginal means of correlations obtained with different decomposition methods and real SSVEP data.

Contrast	500	1000	2000	3000
IFD - LFD	-0.334***	-0.237***	-0.153***	-0.137***
IFD - PFD	-0.443***	-0.308***	-0.196***	-0.175***
LFD - PFD	-0.109***	-0.07***	-0.042***	-0.037***

Signif. codes: <0.001 '***', < 0.01 '**', <0.05 '*', >0.05 n.s.

Table C.23
Estimated marginal means of correlation differences between epoch lengths within different decomposition methods.

Contrast	IFD	LFD	PFD
500 ms. - 1000 ms.	-0.192***	-0.096***	-0.057***
500 ms. - 2000 ms.	-0.342***	-0.161***	-0.095***
500 ms. - 3000 ms.	-0.369***	-0.173***	-0.101***
1000 ms. - 2000 ms.	-0.15***	-0.066***	-0.038***
1000 ms. - 3000 ms.	-0.177***	-0.077***	-0.044***
2000 ms. - 3000 ms.	-0.027, n.s.	-0.011, n.s.	-0.006, n.s..

Signif. codes: <0.001 '***', < 0.01 '**', <0.05 '*', >0.05 n.s.

C.7. Statistical tests comparing decomposition methods, MLR and best Laplacian derivation for each frequency shift estimate applied to real SSVEP data

Table C.24
Interaction and main effects for correlation values obtained using different decomposition methods, MLR and best Laplacian derivation applied to real SSVEP data.

Fr. Est.	Factor	Df	Chisq	Pr(>Chisq)
$\langle f_i \rangle$	Method	2	424.738	< 0.001 ***
	Epoch	3	194.039	< 0.001 ***
	Method:Epoch	6	51.709	<0.001 ***
f_{loc}	Method	2	700.261	< 0.001 ***
	Epoch	3	101.741	< 0.001 ***
	Method:Epoch	6	23.409	<0.001 ***
f_{peak}	Method	2	610.549	< 0.001 ***
	Epoch	3	108.951	< 0.001 ***
	Method:Epoch	6	44.161	<0.001 ***

Signif. codes: <0.001 '***', < 0.01 '**', <0.05 '*', >0.05 n.s.

Table C.25
Estimated marginal means of correlations obtained with different decomposition methods, MLR and best laplacian derivation in real SSVEP data.

Fr. Est.	Contrast	500	1000	2000	3000
$\langle f_i \rangle$	MLR - Lap	0.524***	0.443***	0.351***	0.335***
	MLR - IFD	0.158***	0.125***	0.094***	0.089***
	IFD - Lap	0.366***	0.318***	0.257***	0.246***
f_{loc}	MLR - Lap	0.564***	0.467***	0.395***	0.366***
	MLR - LFD	-0.06**	-0.045**	-0.035**	-0.032**
	LFD - Lap	0.623***	0.512***	0.43***	0.398***
f_{peak}	MLR - Lap	0.527***	0.46***	0.352***	0.332***
	MLR - PFD	-0.224***	-0.175***	-0.117***	-0.109***
	PFD - Lap	0.751***	0.635***	0.469***	0.441***

Signif. codes: <0.001 '***', < 0.01 '**', <0.05 '*', >0.05 n.s.

References

Baillet, S., Mosher, J., Leahy, R., 2001. Electromagnetic brain mapping. IEEE Signal Process. Mag. 18, 14–30.

Benwell, C.S., London, R.E., Tagliabue, C.F., Veniero, D., Gross, J., Keitel, C., Thut, G., 2019. Frequency and power of human alpha oscillations drift systematically with time-on-task. NeuroImage 192, 101–114.

Blankertz, B., Acqualagna, L., Dähne, S., Haufe, S., Schultze-Kraft, M., Sturm, I., Uscumlic, M., Wenzel, M., Curio, G., Müller, K., 2016. The berlin brain-computer interface: Progress beyond communication and control. Frontiers in Neuroscience 10.

Blankertz, B., Tangermann, M., Vidaurre, C., Dickhaus, T., Sannelli, C., Popescu, F., Fazli, S., Danóczy, M., Curio, G., Müller, K.R., 2009. Detecting mental states by machine learning techniques: the berlin brain–computer interface. In: Brain-computer interfaces. Springer, pp. 113–135.

Boashash, B., 1992. Estimating and interpreting the instantaneous frequency of a signal – part 1: Fundamentals. In: In: PROCEEDINGS OF THE IEEE., pp. 520–538.

Bruns, A., 2004. Fourier-, hilbert- and wavelet-based signal analysis: are they really different approaches? Journal of Neuroscience Methods 137 (2), 321–332.

Buzsaki, G., Draguhn, A., 2004. Neuronal oscillations in cortical networks. science 304 (5679), 1926–1929.

Cesnaite, E., Steinfath, P., Jamshidi Idaji, M., Stephani, T., Kumral, D., Haufe, S., Sander, C., Hensch, T., Hegerl, U., Riedel-Heller, S., Röhr, S., Schroeter, M.L., Witte, A., Villringer, A., Nikulin, V.V., 2023. Alterations in rhythmic and non-rhythmic resting-state eeg activity and their link to cognition in older age. NeuroImage 268, 119810.

Cohen, M.X., 2014. Fluctuations in oscillation frequency control spike timing and coordinate neural networks. Journal of Neuroscience 34 (27), 8988–8998.

Dähne, S., Meinecke, F.C., Haufe, S., Höhne, J., Tangermann, M., Müller, K.-R., Nikulin, V.V., 2014. Spoc: A novel framework for relating the amplitude of neuronal oscillations to behaviorally relevant parameters. NeuroImage 86, 111–122.

Dähne, S., Nikulin, V., Ramírez, D., Schreier, P., Müller, K., Haufe, S., 2014. Finding brain oscillations with power dependencies in neuroimaging data. Neuroimage 96, 334–348.

Delorme, A., Makeig, S., 2004. EEGLAB: an open source toolbox for analysis of single-trial eeg dynamics. Journal of Neuroscience Methods 134, 9–21.

Donoghue, T., Haller, M., Peterson, E.J., Varma, P., Sebastian, P., Gao, R., Noto, T., Lara, A.H., Wallis, J.D., Knight, R.T., et al., 2020. Parameterizing neural power spectra into periodic and aperiodic components. Nature neuroscience 23 (12), 1655–1665.

Douma, J.C., Weedon, J.T., 2019. Analysing continuous proportions in ecology and evolution: A practical introduction to beta and dirichlet regression. Methods in Ecology and Evolution 10 (9), 1412–1430.

Evans, A.C., Kamber, M., Collins, D.L., Mac Donald, D., 1994. An mri-based probabilistic atlas of neuroanatomy. In: Shorvon, S.D., Fish, D.R., Andermann, F., Bydder, G.M., Stefan, H. (Eds.), Magnetic Resonance Scanning and Epilepsy. Springer US, Boston, MA, pp. 263–274.

Freeman, W.J., 2004. Origin, structure, and role of background eeg activity. part 2. analytic phase. Clinical Neurophysiology 115 (9), 2089–2107.

Gammaitoni, L., Nov 1995. Stochastic resonance and the dithering effect in threshold physical systems. Phys. Rev. E 52, 4691–4698. doi:10.1103/PhysRevE.52.4691.

Gasser, T., Verleger, R., Bächer, P., Sroka, L., 1988. Development of the eeg of school-age children and adolescents. i. analysis of band power. Electroencephalography and Clinical Neurophysiology 69 (2), 91–99.

Gundlach, C., Müller, M.M., Hoff, M., Ragert, P., Nierhaus, T., Villringer, A., Sehm, B., 2020. Reduction of somatosensory functional connectivity by transcranial alternating current stimulation at endogenous mu-frequency. NeuroImage 221, 117175.

Haegens, S., Cousijn, H., Wallis, G., Harrison, P.J., Nobre, A.C., 2014. Inter- and intra-individual variability in alpha peak frequency. NeuroImage 92, 46–55.

Hashemi, A., Cai, C., Kutyniok, G., Müller, K.-R., Nagarajan, S.S., Haufe, S., 2021. Unification of sparse bayesian learning algorithms for electromagnetic brain imaging with the majorization minimization framework. NeuroImage 239, 118309.

Haufe, S., Dähne, S., Nikulin, V.V., 2014. Dimensionality reduction for the analysis of brain oscillations. NeuroImage 101, 583–597.

Haufe, S., Meinecke, F., Görgen, K., Dähne, S., Haynes, J.-D., Blankertz, B., Bießmann, F., 2014. On the interpretation of weight vectors of linear models in multivariate neuroimaging. Neuroimage 87, 96–110.

Hülsdünker, T., Mierau, A., Strüder, H.K., 2016. Higher balance task demands are associated with an increase in individual alpha peak frequency. Frontiers in Human Neuroscience 9, 695.

Idaji, M.J., Müller, K.-R., Nolte, G., Maess, B., Villringer, A., . Nikulin, V.V., 2020. Nonlinear interaction decomposition (nid): A method for separation of cross-frequency coupled sources in human brain. NeuroImage 211, 116599.

Iemi, L., Gwilliams, L., Samaha, J., Auksztulewicz, R., Cycowicz, Y.M., King, J.-R., Nikulin, V.V., Thesen, T., Doyle, W., Devinsky, O., Schroeder, C.E., Melloni, L., Haegens, S., 2022. Ongoing neural oscillations influence behavior and sensory representations by suppressing neuronal excitability. NeuroImage 247, 118746.

Iscan, Z., Nikulin, V., 01 2018. steady state visual evoked potential (ssvep) based brain-computer interface (bci) performance under different perturbations. PLOS ONE 13(1), 1–17.

Jorajuría, T., Gómez, M., Vidaurre, C., 2020. A fast ssvep-based brain-computer interface. In: International Conference on Hybrid Artificial Intelligence Systems. Springer, pp. 49–60.

Jorajuría, T., Idaji, M.J., İşcan, Z., Gómez, M., Nikulin, V.V., Vidaurre, C., 2021. Oscillatory source tensor discriminant analysis (ostda): a regularized tensor pipeline for ssvep-based bci systems. Neurocomputing.

Lechinger, J., Bothe, K., Pichler, G., Michitsch, G., Donis, J., Klimesch, W., Schabus, M., 2013. Crs-r score in disorders of consciousness is strongly related to spectral eeg at rest. Journal of Neurology 260 (9), 2348–2356.

Lundqvist, M., Bastos, A.M., Miller, E.K., 2020. Preservation and changes in oscillatory dynamics across the cortical hierarchy. Journal of Cognitive Neuroscience 32 (10), 2024–2035.

Mahjoory, K., Schoffelen, J.-M., Keitel, A., Gross, J., 2020. The frequency gradient of human resting-state brain oscillations follows cortical hierarchies. eLIFE 9, e53715.

Maurer, U., Brem, S., Liechti, M., Maurizio, S., Michels, L., Brandeis, D., 2015. Frontal midline theta reflects individual task performance in a working memory task. Brain topography 28 (1), 127–134.

Michel, C.M., Murray, M.M., Lantz, G., Gonzalez, S., Spinelli, L., . de Peralta, R.G., 2004. Eeg source imaging. Clinical neurophysiology 115 (10), 2195–2222.

Mierau, A., Klimesch, W., Lefebvre, J., 2017. State-dependent alpha peak frequency shifts: Experimental evidence, potential mechanisms and functional implications. Neuroscience 360, 146–154.

Nelli, S., Itthipuripat, S., Srinivasan, R., Serences, J.T., 2017. Fluctuations in instantaneous frequency predict alpha amplitude during visual perception. Nature Communications 8 (1), 2017.

Nierhaus, T., Vidaurre, C., Sannelli, C., Müller, K.-R., Villringer, A., 2021. immediate brain plasticity after one hour of brain-computer interface (bci). The Journal of Physiology 599 (9), 2435–2451. doi:10.1113/jp278118.

Nikulin, V.V., Nolte, G., Curio, G., 2011. A novel method for reliable and fast extraction of neuronal eeg/meg oscillations on the basis of spatio-spectral decomposition. Neuroimage 55 (4), 1528–1535.

Nolte, G., 2011-2023. sfb 936 meg & eeg toolbox (s-meth). https://www.sfb936.net/sfb-936-toolbox.

Nolte, G., Dassios, G., 2005. Analytic expansion of the eeg lead field for realistic volume conductors. Phys. Med. Biol 50, 3807–3823.

Nunez, P., Srinivasan, R., 2006. Electric Fields of the Brain: The Neurophysics of EEG. Oxford University Press. 2nd Edition

Oostenveld, R., Fries, P., Maris, E., Schoffelen, J.M., 2011. Fieldtrip: Open source software for advanced analysis of MEG, EEG, and invasive electrophysiological data. Computational Intelligence and Neuroscience 2011, 156869.

Parra, L., Spence, C., Gerson, A., Sajda, P., 2005. Recipes for the linear analysis of eeg. Neuroimage 28, 326–341.

Pascual-Marqui, R.D., Lehmann, D., Koukkou, M., Kochi, K., Anderer, P., Saletu, B., Tanaka, H., Hirata, K., John, E., Prichep, L., Biscay-Lirio, R., Kinoshita, T., 2011. Assessing interactions in the brain with exact low-resolution electromagnetic tomography. Philos Trans A Math Phys Eng Sci 369 (1952), 3768–3784.

Samaha, J., Postle, B.R., 2015. The speed of alpha-band oscillations predicts the temporal resolution of visual perception. Current Biology 25 (22), 2985–2990.

Sameni, R., Seraj, E., 2017. A robust statistical framework for instantaneous electroencephalogram phase and frequency estimation and analysis. Physiological Measurement 38 (12), 2141–2163.

Sannelli, C., Vidaurre, C., Müller, K.-R., Blankertz, B., 2011. Csp patches: an ensemble of optimized spatial filters. an evaluation study. Journal of Neural Engineering 8 (2), 025012.

Schaworonkow, N., Nikulin, V.V., 2022. Is sensor space analysis good enough? spatial patterns as a tool for assessing spatial mixing of eeg/meg rhythms. Neuroimage 253, 119093.

Searle, S.R., Speed, F.M., Milliken, G.A., 1980. Population marginal means in the linear model: An alternative to least squares means. The American Statistician 34 (4), 216–221.

Srinivasan, R., Bibi, F.A., Nunez, P.L., 2006. Steady-state visual evoked potentials: distributed local sources and wave-like dynamics are sensitive to flicker frequency. Brain topography 18 (3), 167–187.

Stephani, T., Hodapp, A., Jamshidi Idaji, M., Villringer, A., Nikulin, V.V., 2021. Neural excitability and sensory input determine intensity perception with opposing directions in initial cortical responses. eLife 10, e67838.

Sutherland, C., Doiron, B., Longtin, A., 2009. Feedback-induced gain control in stochastic spiking networks. Biological Cybernetics 100 (6), 475.

Team-R-Core, 2018. R: A language and environment for statistical computing 2014. R Foundation for Statistical Computing: Vienna, Austria.

Thut, G., Nietzel, A., Brandt, S.A., Pascual-Leone, A., 2006. α-band electroencephalographic activity over occipital cortex indexes visuospatial attention bias and predicts visual target detection. Journal of Neuroscience 26 (37), 9494-9502.

Tuckwell, H., Jost, J., Gutkin, B., 09 2009. inhibition and modulation of rhythmic neuronal spiking by noise. Physical review. E, Statistical, nonlinear, and soft matter physics 80, 031907.

Tukey, J.W., 1949. Comparing individual means in the analysis of variance. Biometrics 99–114.

Valdés-Hernández, P.A., Ojeda-González, A., Martínez-Montes, E., Lage-Castellanos, A., Viués-Alba, T., Valdés-Urrutia, L., Valdes-Sosa, P.A., 2010. White matter architecture rather than cortical surface area correlates with the eeg alpha rhythm. NeuroImage 49 (3), 2328–2339.

Van Veen, B.D., Van Drongelen, W., Yuchtman, M., Suzuki, A., 1997. Localization of brain electrical activity via linearly constrained minimum variance spatial filtering. IEEE Transactions on biomedical engineering 44 (9), 867–880.

Vidaurre, C., Haufe, S., Jorajuría, T., Müller, K.-R., Nikulin, V.V., 2020. Sensorimotor functional connectivity: a neurophysiological factor related to bci performance. Frontiers in Neuroscience 1278.

Vidaurre, C., Jorajuría, T., Ramos-Murguialday, A., Müller, K.R., Gómez, M., Nikulin, V.V., 2021. Improving motor imagery classification during induced motor perturbations. Journal of neural engineering 18 (4), 0460b1.

Vidaurre, C., Murguialday, A.R., Haufe, S., Gómez, M., Müller, K.-R., Nikulin, V.V., 2019. Enhancing sensorimotor bci performance with assistive afferent activity: an online evaluation. Neuroimage 199, 375–386.

Vidaurre, C., Nolte, G., de Vries, I.E., Gómez, M., Boonstra, T.W., Müller, K.-R., Villringer, A., Nikulin, V.V., 2019. Canonical maximization of coherence: a novel tool for investigation of neuronal interactions between two datasets. Neuroimage 201, 116009.

Vidaurre, C., Pascual, J., Ramos-Murguialday, A., Lorenz, R., Blankertz, B., Birbaumer, N., Müller, K.R., 2013. Neuromuscular electrical stimulation induced brain patterns to decode motor imagery. Clinical Neurophysiology 124 (9), 1824–1834.

Ville, J., 1948. Theorie et application dela notion de signal analytique. Câbles et transmissions 2 (1), 61–74.

Zeileis, A., Cribari-Neto, F., Gruen, B., Kosmidis, I., Simas, A. B., Rocha, A. V., Zeileis, M. A., Package 'betareg'. R package2016. 3, 2.

Zimmermann, R., Gschwandtner, U., Wilhelm, F.H., Pflueger, M.O., . Riecher-Rössler, A., Fuhr, P., 2010. Eeg spectral power and negative symptoms in at-risk individuals predict transition to psychosis. Schizophrenia Research 123 (2), 208–216.